UNIVERSITY OF KWAZULU-NATAL (HOWARD COLLEGE)

MASTERS THESIS

Discrete Energy Minimisation Optimisation using Graph Cuts for Fluorescence Microscopy

Author:
Ryan NAIDOO

Supervisor:
Dr. Jules-Raymond TAPAMO

A thesis submitted in fulfillment of the requirements
for the degree of Master of Science in Engineering

in the

Department of Electrical, Electronic and Computer Engineering
School of Engineering

October 3, 2016

Declaration of Authorship

I, Ryan NAIDOO, declare that this thesis titled, "Discrete Energy Minimisation Optimisation using Graph Cuts for Fluorescence Microscopy" and the work presented in it are my own. I confirm that:

- This work was done wholly or mainly while in candidature for a research degree at this University.

- Where any part of this thesis has previously been submitted for a degree or any other qualification at this University or any other institution, this has been clearly stated.

- Where I have consulted the published work of others, this is always clearly attributed.

- Where I have quoted from the work of others, the source is always given. With the exception of such quotations, this thesis is entirely my own work.

- I have acknowledged all main sources of help.

- Where the thesis is based on work done by myself jointly with others, I have made clear exactly what was done by others and what I have contributed myself.

Signed:

Date:

"Thanks to my solid academic training, today I can write hundreds of words on virtually any topic without possessing a shred of information, which is how I got a good job in journalism."

Dave Barry

UNIVERSITY OF KWAZULU-NATAL (HOWARD COLLEGE)

Abstract

Faculty of Engineering
School of Engineering

Master of Science in Engineering

Discrete Energy Minimisation Optimisation using Graph Cuts for Fluorescence Microscopy

by Ryan NAIDOO

The Thesis Abstract is written here (and usually kept to just this page). The page is kept centered vertically so can expand into the blank space above the title too...

Acknowledgements

The acknowledgments and the people to thank go here, don't forget to include your project advisor...

Contents

List of Figures

List of Tables

List of Algorithms

List of Abbreviations

ACWE	Active Contours Without Edges
AOD	Average Optical Density
BCC	Boundary Chain Code
BFS	Breadth First Search
BP	Belief Propagation
CCD	Charge-Coupled Device
CED	Coherence Enhancing Diffusion
CLSM	Confocal Laser Scanning Microscopy
CRF	Conditional Random Field
DCC	Differential Chain Code
DFS	Depth First Search
DNA	Deoxyribonucleic Acid
DP	Dynamic Programming
DT	Delaunay Triangulation
EGFP	Enhanced Green Fluorescent Protein
EM	Expectation Maximisation
FCS	Fluorenscence Correlation Spectroscopy
FIFO	First-In First-Out
FISH	Fluorenscence in-situ Hybridisation
FLIM	Fluorenscence Lifetime Imaging Microscopy
FRAP	Fluorenscence Recovery After Photobleaching
FRET	Fluorenscence Resonance Energy Transfer
GA	Genetic Algorithm
GFP	Green Fluorescent Protein
GLCM	Gray Level Co-occurrence Matrix
GMM	Guassian Mixture Modelling
GRF	Gibbs Random Field
HLF	Highest Level First
ICC	Immunocytochemistry
ICF	Immunocytofluorescence
ICM	Iterated Conditional Modes
IHC	Immunohistochemistry
IHF	Immunohistofluorescence
IOD	Integrated Optical Density
Laser	Light Amplification by Stimulated Emission of Radiation
LBP	Loopy Belief Propagation
LED	Light Emitting Diode
LoG	Laplacian of Gaussian
MAP	Maximum A Posteriori
MIS	Medical Image Segmentation
MLP	Multi-Layered Perceptron

MRF	**M**arkov **R**andom **F**ield
MST	**M**inimum **S**panning **T**ree
NA	**N**umerical **A**perture
ORI	**O**ptimised **R**otational **I**nvariance
OTF	**O**ptical **T**ransfer **F**unction
PSF	**P**oint **S**pread **F**unction
RF	**R**andom **F**ield
RNA	**R**ibo**n**ucleic **A**cid
SNR	**S**ignal-to-**N**oise **R**atio
TV	**T**otal **V**ariation
UV	**U**ltra**v**iolet

Physical Constants

Speed of Light	$c = 2.997\,924\,58 \times 10^8\,\mathrm{m\,s^{-1}}$ (exact)
Planck's Constant	$h = 6.626\,070\,04 \times 10^{-34}\,\mathrm{m^2\,kg\,s^{-1}}$ (exact)

List of Symbols

a	distance	m
P	power	$W\ (J\,s^{-1})$
ω	angular frequency	rad

For/Dedicated to/To my…

Chapter 1

Introduction

1.1 Literature Review

The Literature Review is here.

1.2 Outline and Contributions

The introduction is here.

1.3 Thesis Overview

The remainder of the thesis outline.

Chapter 2 is where we cover the mathematical foundation to Graph Cut image segmenation.

Chapter 3 is where we cover the mathematical foundation to Graph Cut image segmenation.

Chapter ?? is where we cover the mathematical foundation to Graph Cut image segmenation.

Chapter ?? is where we cover the mathematical foundation to Graph Cut image segmenation.

Chapter ?? is where we cover the mathematical foundation to Graph Cut image segmenation.

Chapter 4 is where we cover the mathematical foundation to Graph Cut image segmenation.

Chapter 5 concludes the thesis with suggestions for further work.

Chapter 2

Fluorescence Microscopy

What is fluorescence microscopy? What's it's purpose in the thesis? Photoluminescence -> fluorescence and phosphorescence. Discovery of fluorescence: Brief history and evolution. Brief discussion on the remainder of the chapter. Fluorescence microscopy has become an essential tool in diverse fields, such as petrology, semiconductors, etc, and has especially been established as a choice imaging technique in cellular and molecular biology for visualisation of cells and tissues [1–5]. In this thesis we confine our attention to its use in cellular biology.

Certain substances emit radiation when irradiated with a higher intensity light, such as ultraviolet (UV), blue or green, which is off a longer wavelength than that of the exciting light, this is known as *Stokes' Law*. This phenomenon is known as *photoluminescence* [6–9]. There are two types of photoluminescence. If emission persists at an appreciable level after the exciting light is turned off, then we call this *phosphorescence*. If emission persist only so long as the exciting light is on, then we call this *fluorescence* [6, 10].

The first observance and publishing of fluorescence is credited to Sir John Frederick William Herschel around 1852. In 1852, Sir John George Stokes published a 100 page treatise about this luminescent phenomenon and coined the term *fluorescence*, over Herschel's *dispersive reflection*, when he observed that the mineral *fluorite* emitted red light when irradiated by ultraviolet (UV) light [2, 11].

In the remainder of this chapter we present the underlying principles of fluorescence, how specimens are fluorescently marked, the optical principles of microscope design, image acquisition, image processing and common analysis in cellular biology. We only go so far in depth as to present a rudimentary understanding of fluorescence microscopy as is necessary for the comprehension of this thesis.

2.1   Physics of Fluorescence

Why is it necessary to understand the principles of fluroescence? Simple description of the fluorescence process. A more in-depth explanation of the fluorescence process and why stuff goes wrong e.g. phosphorescence, fading, etc. Fluorescence microscopy is a cross-disciplinary field. It is encouraged, if not necessary, to have a photophysical understanding of the principles of fluorescence, for biologists and computer scientists. The knowledge of the "under the hood" mechanics of fluorescence empower computer scientists to make informed and directed research in terms of image processing. The aim here is to present an elementary introduction into the physics of fluorescence.

The overall principle of fluorescence can be explained in three steps [12] as illustrated in 2.1(a): (1) Energy is absorbed by an atom upon collision with a photon. (2) The atom becomes excited and an electron jumps to a higher energy level. (3) Shortly after jumping to the higher energy level the electron returns to the ground state and emits a photon.
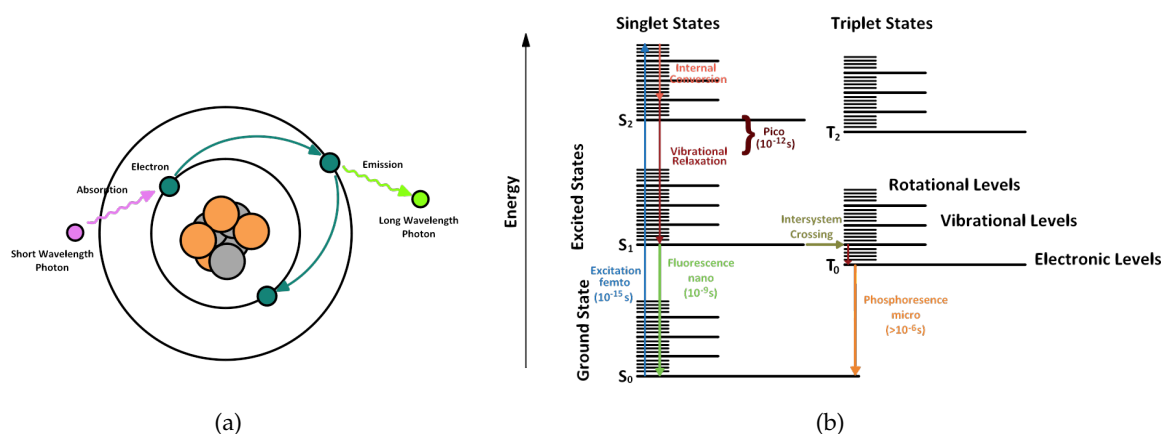
FIGURE 2.1: **(a)** Simplified fluorescence process. **(b)** The Jabłoński diagram depicting the electronics states from photon absorption to photo emission.

Excitation and emission One of the best ways to visualise the fluorescing process is using a Jabłoński diagram. A detailed Jabłoński diagram is shown in 2.1(b). When a photon collides with an atom, all its energy is transferred to the atom. The energy of the photon is inversely related to it's wavelength, $E = h\frac{c}{\lambda}$, where h is Planck's constant and c and λ are the speed and wavelength of light in a vacuum respectively. This increase in energy moves an electron from the ground state S_0 to a higher level energy state. Depending on the energy of the photon and the number of photons absorbed by the photon the electron can move to different energy levels e.g. S_1, S_2, etc. This process happens almost immediately in the order of femtoseconds($10^{-15}s$). Before moving to the lowest next higher energy level (S_1), some energy is lost due to internal conversion and vibrational relaxation. When the electron spontaneously decays from S_1 to S_0 it emits a photon of longer wavelength than the absorption photon. This happens few nanoseconds ($10^{-9}s$) after excitation.

   The difference in wavelength of the emission photon and excitation photon is known as the *Stokes' Shift* or *Stokes' Law*. The larger the Stokes' Shift the easier it is to separate the emission light from the excitation light [1]. The emission curve is often a mirror image and shifted to longer wavelengths than the excitation curve as illustrated in Figure 2.2.

Fluorophores Substances that exhibit the fluorescent property are called fluorophores, also known as *fluorochromes* or *fluoresent dyes*. Early investigations showed that many substance naturally posess fluorescent properties, such as minerals, crystals, resins, crude drugs, butter, chlorophyll, vitamins, etc [1]. This is known as *autofluorescence*. Substances that do not fluoresce must be *stained* such that it can be observed through a fluorescent microscope, more on this later.

Intersystem crossing If the electron spin as the electron transfer between energy states is preserved then the energy states are known as *singlet states*. It is also possible for the electron to reverse it's spin. This is very unlikely and is known as *forbidden transition* in Quantum mechanics. When this happens the electron is said to be in a *triplet state*, see 2.1(b). The only way for the electron to reach the ground state is to again undergo another forbidden transition which is unlikely. When this does eventually happen the electron may emit a photon and this phenomenon is known as *phosphorescence*. This process takes much longer, in the order of microseconds ($10^{-6}s$).
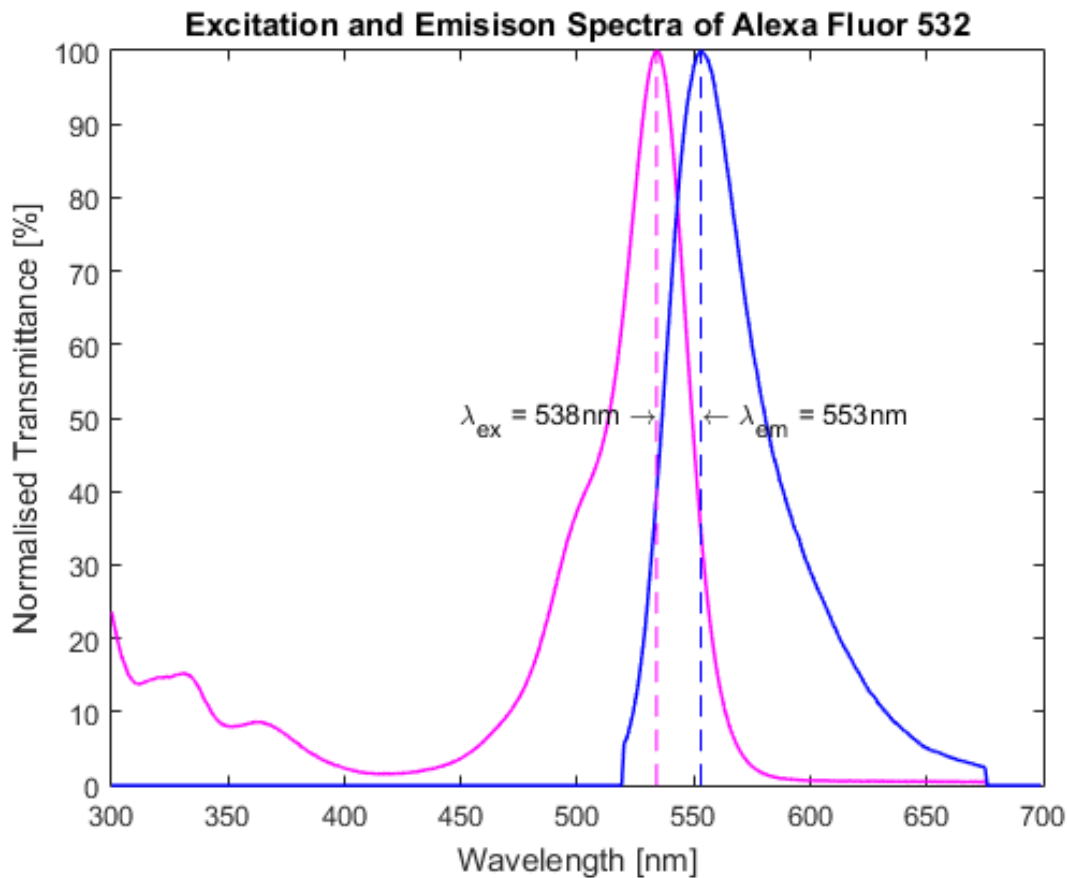
FIGURE 2.2: Normalised Excitation and Emmision Spectra of the Alexa Fluor 532 flurophore. The emmission maximum is at $553nm$ which is a more yellow-green than excitation maximum at $5534nm$. Data obtained from ThermoFisher Scientific [13].

2.2   Specimen Labelling

Why do specimens have to be stained? What is is staining? Many of the components of interest, such as cell nuclei, cytoplasm, genes, chrosomes, proteins, do not possess a high degree of, if not any, autofluorescence. In this scenario, these components can be marked with a fluorescent dye [14], also known as a fluorophore or fluorochrome, a substance that can bind to a specific target whose excitation and emission spectra are well known. This is known as staining [2, 3, 11]. Once the specimen is stained it can be indirectly observed using a fluorescence microscope.

What are the most common staining protocols? The most prevalent staining techniques are fluorescence in-situ hybridisation (FISH) and immunostaining [2, 4, 15, 16].

FISH staining What is FISH? What is the FISH staining techniques used for? FISH is a molecular cytogenetic technique that uses flourophores that bind to selected regions in nucleic acids [2, 4]. FISH is the most frequently used staining technique used primarily for visualisation and localisation of nucleic acid sequences, chromosomes, cytplasm or organelles which contain those acids [3]. This makes FISH highly attractive for finding specific features in DNA and RNA used in genetic diagnosis and research, medicine and species identification [4, 17]. Figure 2.3(a) is a capture of mouse chromosomes using the FISH staining technique.

Immunostaining What is Immunofluorescence and the two main types, what is the difference between the two, and which is more common? What is the Immunofluorescence staining techniques used for? Immunofluorescence is the detection method where an antibody is used to detect an antigen in a tissue or a cell using fluorescence. Flourophores are usually conjugated onto antibodies, which are proteins that are designed bind to specific antigens, target proteins, on a cell [18]. The two types of immunofluorescent detection are immunocytofluorescence (ICF) and immunohystofluorescence (IHF). It must not be confused with immunocytochemistry (ICC) and immunohistochemistry (IHC). *Immuno* refers to the immunological technique, i.e. the binding of antibodies to antigens. *Cyto* refers to cells, i.e. cells without the extracellular membrane. *Histo* refers to tissue i.e. cells with the extracellular membrane. *Chemistry* refers to the chemical method of detection, e.g. a change in colour. *Fluorescence* detection by emission of light [19]. Figure 2.3(b) shows the detection of the p53 Binding Protein 1 in perfusion fixed frozen sections of rat kidney.

Live-cell staining FISH and IHC cannot stain live cells. Why? How can we stain live cells? The previously discussed staining techniques are not suitable to observe living cells. The fluorescent dyes used are phototoxic and cause cells to die. The circumvent this problem an elegant solution has been devised. Instead of staining, the cells are modified to produce a fluorescent substance in the target structures. Derivatives of the *green fluorescent protein* (GFP), isolated from the *Aequorea victoria* jellyfish [4, 14, 20], are used as it generates a strong photon emission and is non-toxic to living cells [2, 3, 11].

Important notes about fluorophores and the impact on image quality?

2.3   The Epifluorescence Microscope and Image Acquisition

What is a fluorescent microscope? Schematic layout of a fluorescence microscope? Function and purpose of each component in the fluorescent microscope? A fluorescence microscope is an optical microscope that is designed specifically to exploit the principle of fluorescence to allow for the observation of flourescently labelled specimens [3, 4, 8, 11, 21]. There are many types of fluorescent micrcoscopes avaialble but the favoured type among many biologists and geneticists is the epifluorescent microscope [9, 22]. The schematic of the epifluorescent micrcoscope is illustrated in Figure 2.4.

Light source What sort of light needs to be generated? What sort of lamps are used? Advantages and disadvantages of certain lamps. The light source is typically a high-luminance light source e.g. Mercury or Xenon arc lamps, LEDs, lasers, etc [2, 3, 22–24]. The primary criterion for choosing a light sources is that its characeristic peaks must coincide with the excitation spectrum of the fluorophores being used [1, 4, 20]. Wavelength coverage spans from near infra-red to UV. Mercury and Xenon arc lamps are expensive, an inexpensive and lightweight alternative is bright LEDs [4, 6, 11, 23].

Excitation filter What is an excitation filter? Why is it needed? The incoming light from the light source is typically mulispectral [10]. The excitation filter is a wavelength selection filter which is placed in the path of the incoming light and filters through only those wavelengths in the absorption spectrum of the fluorescent dye [1–4, 11, 18, 20, 24].

Dichroic mirror What is a dichroic mirror? Why is it needed? Also known as a *dichroic beam splitter*. This is placed at a 45° angle and reflects the short-wavelenght light filtered through the

(a)

(b)
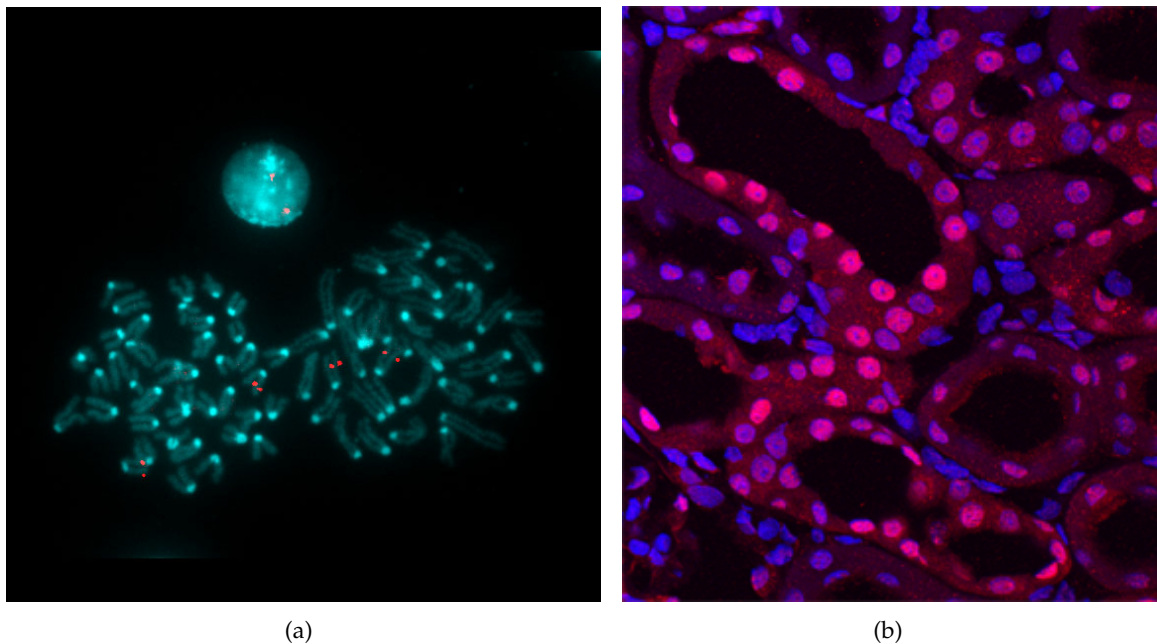
FIGURE 2.3: **(a)** FISH (Fluorescent 'in-situ' Hybridization) in mouse chromosomes using a BAC clone labeled with Spectrum Orange. The picture shows two metaphases and one interphase with two signals in each exampling a homozygous mouse for a transgenic clone. Image Source: "All About the Human Genome Project" Genetic and Genomic Image and Illustration Database. **(b)** p53 Binding Protein 1 (53BP1) was detected in perfusion fixed frozen sections of rat kidney using Goat Anti-Human 53BP1 Antigen Affinity-purified Polyclonal Antibody (Catalog # AF1877) at 15 μg/mL overnight at 4°C. Tissue was stained using the NorthernLights^{TM}557-conjugated Anti-Goat IgG Secondary Antibody (red; Catalog # NL001) and counterstained with DAPI (blue). Specific staining was localized to nuclei of epithelial cells in convoluted tubules. Image Source: R&D Systems' IHC image database.
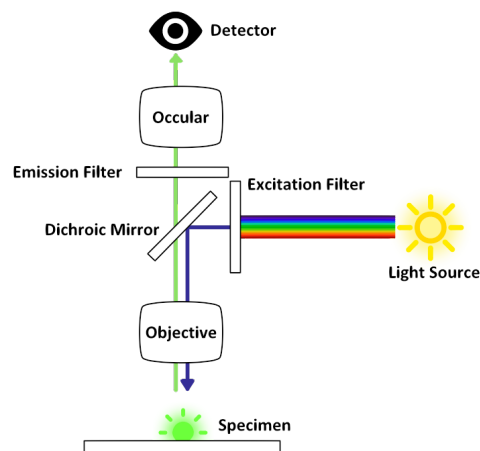
FIGURE 2.4: The schematic of the epifluorescence microscope.

excitation filter at a 90° angle towards the specimen [1–3, 18] and allows the long-wavelength light from the fluorescing specimen to pass through to the detector [6, 20], thus serving as a separation filter between the absorption and emission light [4, 11].

Objective What is the objective? Why is it needed? The incoming light reflected of the

dichroic mirror passes through the objective lens before reaching the specimen [1–3, 20]. Emission light from the fluorescing specimen is gathered in the objective lens and passed through to the dichroic mirror.

Specimen Say something about the specimen, for wholeness sake. The specimen is irradiated by the incoming light from the objective and emits long-wavelength light in all directions. The specimen is stained with a flourophore whose absorption and emission curves are well known. This is important since the light source and the interference filters are chosen using the peaks of these curves.

Emission filter What is an emission filter? Why is it needed? Also known as a *barrier filter* [1, 6, 20]. The light coming from the specimen contains multiple wavelengths and the dichroic mirror is used to filter out the shorter wavelength light. The emission filter is further used to filter out the wavelengths that correspond to the emission wavelengths of the fluorophore [2, 3, 10, 18, 24].

Detector What is the detector why is it needed? The dector is used to capture the emission light and can further digital form the image. The detector is usually a photodector such as a CCD (charge-coupled device) camera or a photomultipler tube [1–3, 20, 25]. It is vital that an appropriate detector be chosen as this has direct impact on image quality [4].

Other Types of Fluorescence Microscopes: Confocal, TIRF. Acquisition: CCD, Hardware setup effect on image quality, Numerical Aperture, Sub-diffraction The type of fluorescence image data that needs to be captured is application dependant and this impacts the decision on which type of microscope to use. The *widefield*, or conventional, microscope produces 2D image data. 3D image data cannot be captured directly. Instead, a series od 2D images are captured to form a 2D stack. The 3D image is then constructed in software. In this scenario, the most common choice of micrscope is the *confocal laser scanning microscope* (CLSM). This microscope system is expensive and acquisition is slower. An economical alternative is the *confocal spinning disk miscroscope*. To detect single molecules, the favoured technique is *total internal reflection fluorescence* (TIRF) which can be achieved by a modification of the epifluorescence micrcoscope.

2.4   Image Processing

Limitations in Fluorescence Imaging. Preprocessing: Point Spread Function deconvolution, etc. Segmentation Due to the physical nature of the fluorescence and image acquisition process, there are many factors that can degrade image quality. There are measures that can be taken to largely mitigate some problems but they can never be completely abated. The presence of these factors directly affect segmentation accuracy and subsequently higher level analysis. Therefore, images are processed prior to segmentation to suppress the artefacts and reconstruct the original data [2] or better yet enhance it. Chapter 4 takes a step in this vain. Here we present some of the commonly occuring factors that reduce image quality and the methods used to mitigate them, and some of the techniques employed for segmentation.

2.4.1   Preprocessing

Write a little something on preprocessing.
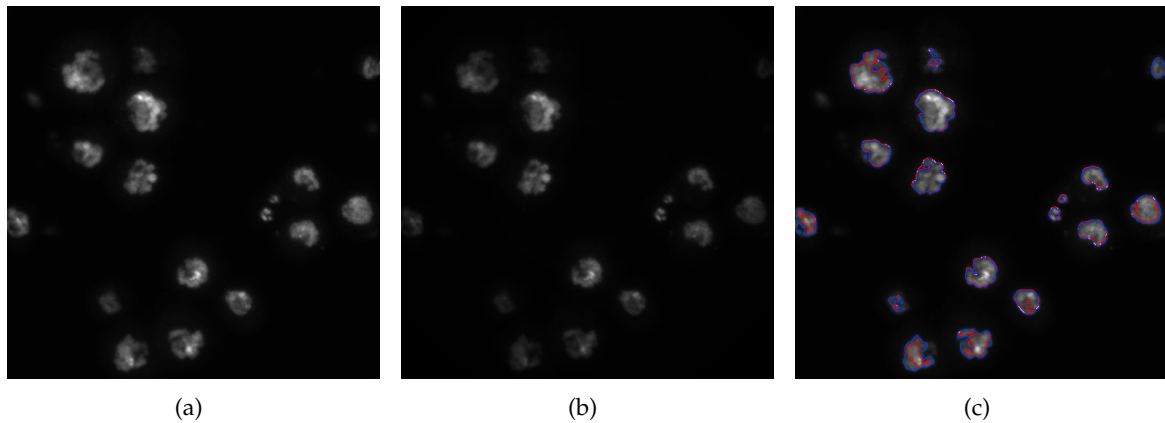
FIGURE 2.5: The effect of nonuniform illumination on segmentation. **(a)** Original image. Image source: The Cell Image Library [30]. **(b)** Nonuniformly illuminated image. The Vignette effect. **(c)** K-means clustering using the Euclidean distance metric and 2 clusters. The blue curve is from the original, the red curve is from the nonuniformly illuminated image. Notice that less of the object is recognised towards the edges.

Nonuniform illumination What causes uneven illumination? What techniques are done to reduce it's effect. Vignette effect, etc. There are many factors that could contribute to nonuniform illumination. The specimen layer will not be uniformly lit if the arc lamp is not properly focussed on the black aperture. To prevent this from happening, a liquid light guide-based light source, which provide even illumination may be used [20]. If the light brightness diminished towards the edges of the image then this is known as the *Vignette effect*. Common techniques to suppress this distortion is *background correction*, also known as *flat-field correction*, *background flattening* or *shading correction* [2, 4, 25]. Other causes of nonuniform illumination are inhomogenous detector sensitivity, autofluorescence, dirt particles in the optical system or nonspecific sample staining. An example of the Vignette effect is illustrated in 2.5(b). Computational schemes to eliminate nonuniform illumination have been well researched, although recently it hasn't recived too much attention [26–29].

Fading What causes quenching and bleaching? What techniques are done to reduce it's effect. Why is photobleaching worse? The reduction of emission intensity is called *fading*, of which there are two types: *quenching* and *bleaching*.

Quenching is a reversible loss of fluorescence owing to a variety of nonradiative energy-loss mechanisms such as collisions with nearby acceptor molecules, a phenomenon known as *resonance energy transfer*. This phenomenon is useful in studying molelcular interactions below the lateral resolution of the light microscope through a technique called *fluorescence resonance energy transfer* (FRET) [1, 2, 20].

Bleaching refers to all processes that cause a fluorescent signal to fade permanently [20]. From the fluorescence process presented in Section 2.1, one may assume that, under the proper conditions, a fluorochrome has the ability to fluoresce indefinitely. However, this is not the case. There is a limit number of cycles before permanent bleaching [20]. Figure 2.6 illustrates the effect of photobleaching. *Photobleaching* is the most prominent form of bleaching. It is due the interaction of the fluorophore with an oxygen molecule. This can move the oxygen molecule to an excited singlet state, which then becomes a reactive molecule. When in this state, the oxygen molecule can participate in many chemically destructive reaction with
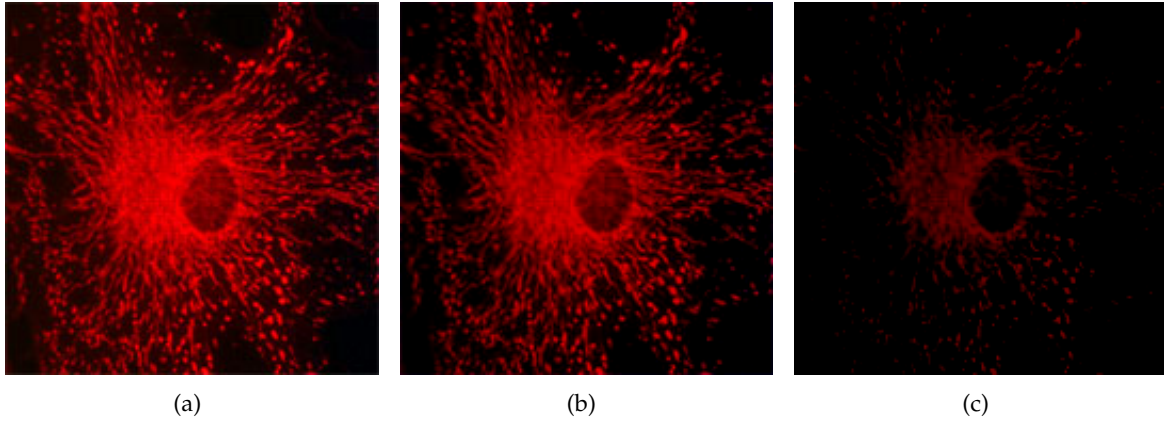
FIGURE 2.6: The effect of photobleaching. Image Source: Molecular Expressions [32]. **(a)** Original image at $t = 0s$. **(b)** Image after $t = 10s$. **(c)** Image after $t = 20s$.

organic molecules causing *phototoxicity* [2]. Photobleaching is used to study diffusion and motion through a technique called *fluorescence recovery after photobleaching* (FRAP) [9, 20].

Photobleaching cannot be avoided but it be can pushed back. The aim in the measures to avoid photobleaching is to take a longer time to reach *reciprocity failure* [9]. This is done by shortening exposure times and using less intensive excitation light. This, however, yields low contrast images. These images with low signal-to-noise [25] ratio (SNR) are more difficult to segment hence contrast enhancement must be performed on the images prior to segmentation [31].

Image distortion What causes image distortion (PSF)? What techniques are done to reduce it's effect. The major contributing factors to image distortion are: The *point spread function* (PSF) and noise [8]. Image formation can be approximated by

$$O = n(s \otimes h), \tag{2.1}$$

where O is the formed image, n is the noise function, s is the exact image and h is the specific PSF of the optical system. We discuss the PSF first. The observed image isn't an exact representation of the real object. Optical systems have an inherent property called the point spread function which is the systems optical response to a point light source [2]. The final image is dependant on the spatial position of a point, numerical aperture (NA) and furthermore differs for various emission wavelengths [3, 33]. The final image is a superposition of all points in the illuminated volume where the contribution of each is described by the PSF.

Theoretically the exact image can be obtained by deconvolution of the observed image with the PSF. However, there are secondary factors that prevent this. Deconvolution seeks to reconstruct the original image given the PSF and certain assumptions about noise [33]. This is an *ill-posed problem* as little is known about the specific PSF or the noise model. Additionally, if the image is corrupted by too much of noise, deconvolution might still produce unsatisfactory results. The PSF is generally experimentally determined or theorectically modelled, and so the true PSF is never attained. Hence, the original image can never be attained by deconvolving with an approximated PSF. The image formation and restroration process is illustrated in Figure 2.7.

Deconvolution has recieved a lot of attention in the passed with very creative approaches [35–39]. Fluorescence microscopy deconvolution is still a very active field of research. Bayesian
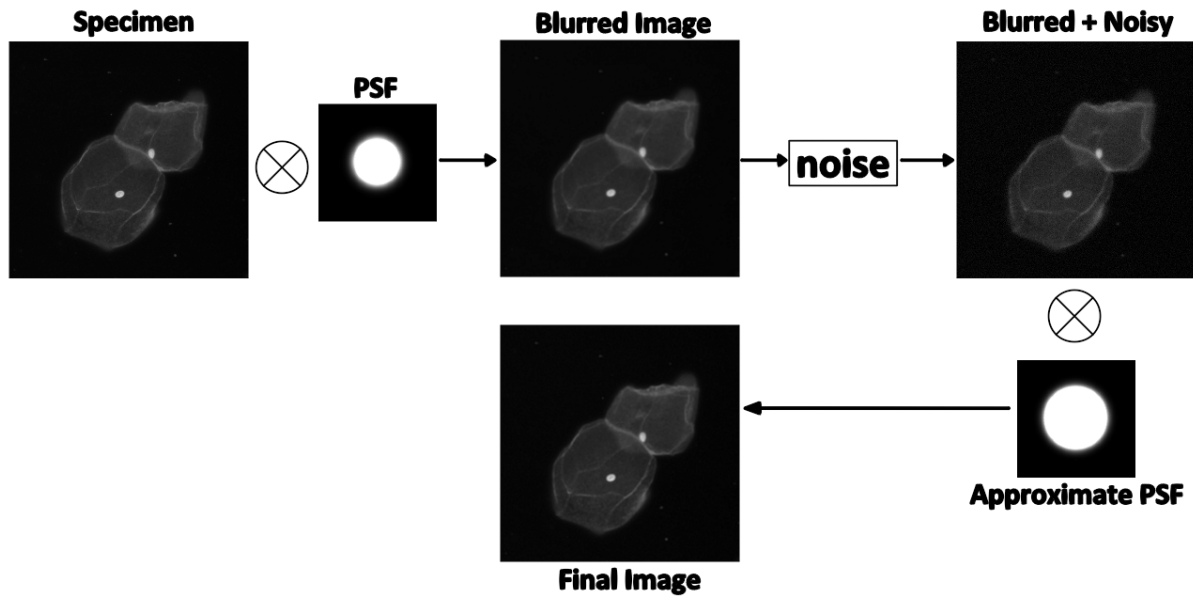
FIGURE 2.7: The image formation process. Image source: [34]

methods have become popular in fluorescence microscopy image deconvolution, however noise in low SNR imaging conditions still poses a challenge [40]. Recent trends in 3D deconvolution in widefield microscopy use blind depth-invariant of the PSF [41]. Most PSF deconvolution systems naïvely assume depth-invariance however, the PSF changes significantly along the optical axis. There are also deconvolution methods that can preserve detail and possibly enhance image quality in diffraction-limited/superresolution imaging modalilities [42].

Noise What types of noise are most prevalent? How do they arise? What techniques are done to reduce it's effect. As previously stated, fluorescence imaging is a low light, low contrast and low SNR imaging technique to counter the effects of bleaching. For these reasons, noise becomes prominent. The three types of noise recorded by a camera is *dark noise*, *read noise* and *photon noise* [2, 3, 5, 11].

The electrons in a CCD of film are always in motion due to thermal energy. Dark current is due to the extraneous electrons which excited into the signal. This signal carries a statistical fluctuation known as dark noise. Dark current effects can be reduced by ground image subtraction or cooling the CCD. If there is a significant amount of dark noise then the background won't be as black as it should be. For this reason it is common to mistake dark noise for low-level autofluorescence [11, 43].

Read noise is a result of the conversion process from charge build-up to a voltage and then digitisation.

Photon noise, also known as *shot noise*, is the signal dependant statical variation of the counting of photons incident on the CCD or film. This is a naturally occuring phenomenon and cannot be reduced by camera design of system optimisation [43].

In low-light imaging techniques, such as is common in fluorescence imaging, the dominant form of noise is photon noise. Photon noise and dark noise are Poisson distributed [2, 43, 44]. Noise is low-light images used to modelled using the Gaussian distribution but was found to be a poor description of the noise. The Poisson distribution provides a more physically accurate model especially in photon-limited recording [8]. We study deonising in Section 4.3. The effect of noise on segmentation accuracy is illustrated in Figure 2.8.

(a)   (b)   (c)
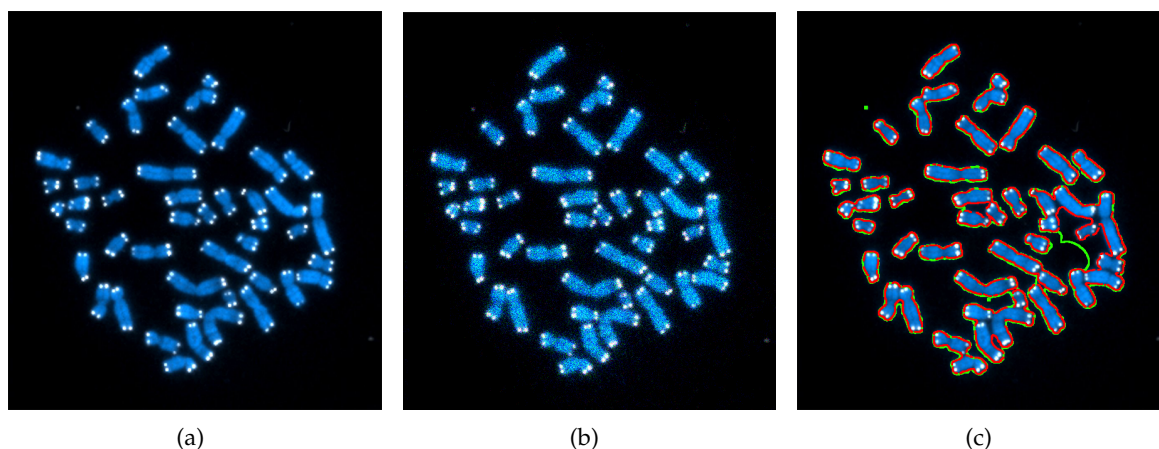
FIGURE 2.8: The effect of noise on segmentation. **(a)** Original image. **(b)** Poisson noise corrupted image. **(c)** ACWE Chan-Vese segmentated output. The red curve is from the original, the green curve is from the Poisson noise corrupted image. Notice that there are more artifacts and the segmented output is less accurate especially towards the bottom left from the green curve.

2.4.2   Segmentation

Write a little something on segmentation in cell imaging. Basic historical track of cell segmentation. Focus on specfic segmentation techniques. The primary aim of using fluorescence microscopy imaging is to make diagnoses and to study molecular behaviour and interaction. This means that biologists, geneticists and other professionals alike, not only have a super-abundance of microscopic imaging techniques at their disposal, but also have an immense amount of image data to analyse since the outburst of image acquisition technology. The abundance, diversity, dimensionality and complexity of fluorescence image data obviates manual image processing as this isn't tractable, by any means, in terms of time or quality [43, 45]. Consequently, the task has fallen to computers to perform these tasks and has now become of essential in advancing these fields [46, 47]. The crux of image analysis lies on the accuracy of image segmentation and has become the principle focus in many studies [48].

Anton van Leeuwenhoek, a Dutch draper and scientist, is credited with the invention of the first real compound microscope in the late 17th century. However, it wasn't until the mid-1950s that computers became involved when systems were developed to automate the classification of smears of exfoliated cells. These systems used simple thresholding rules on 1D scanning of microscopic lines [49]. In the 1960s, automated systems were developed to count leukocytes on 2D image data based on their colour and morphological measurements [50]. In the 1980s the invention of the confocal microscope made it possible to study cells in 3D but it wasn't until the 1990s that computer became powerful enough to process 3D image data or complex 2D images [51]. The trends of increased computing power has made possible the use of more sophisticated cell analysis techniques as well as the ability to use more computationally demanding segmentation methods. The literature on cell segmentation and analysis has experienced exponential growth in the last couple of decades. Many studies comparing segmentation algorithms for cells have been pubished [52–54]. We review some of the common techniques used in fluorescence microscopy image segmentation.

Intensity thresholding Say something about this section. Intensity thresholding assumes a

non-overlapping intensity levels between the objects and the background. It is still one of the most common thresholding methods for cell segmentation [55–57]. Locally adaptive thresholding techniques are used when illumination varies across the image. Automated threshold segmentation techniques are usually based on global or local intensity using the histogram [48]. Thresholding produces suboptimal results due to the naïve assumption of mutually exclusive intensity levels.

Morphological segmentation Say something about this section. This method uses non-linear mathematical morphological operators like erosion, dilation, opening, closing, etc with geometrical and topological properties to segment the image [56, 58–61]. Generally, this method is used as a post-processing step to polish up coarse segmentation or a pre-processing step to suppress certain image structures [48].

Region accumulation Say something about this section. This method starts with selected points, called seeds. The idea is to iteratively add points neighboring previously labelled pixels based on some conformity measure, usually intensity. The most common implementation is called *region growing*. Most cases assume an image model similar to that of thresholding and suffers the same segmented results problems. Another approach is called the *watershed method* which converts the image into an open 3D shape and "fills the shape with water". The different regions are separated by those "filled with water" and those that aren't. A common problem with this method is oversegmentation and usually requires post-processing methods, like *region merging*, to get a meaningful result [48, 62, 63].

Edge-based segmentation Say something about this section. There are basically two types of edge-based segmentation: *gradient based methods* and *Laplacian based methods*.

Gradient methods are based on the assumption that there is a rapid intensity gradient between the object and the background. Edges are detected by searching for the maximum and minimum in the first derivative, e.g. Prewitt, Roberts and Sobel operators.

Laplacian methods search for zero-crossings in the second derivative, e.g. Marr-Hildreth, Laplacian of Gaussian (LoG), Canny edge detection.

These algorithms are very fast to compute but the drawback is when closed curves are desired [48], which is a common criterion in biological and molecular segmentation. A solution to this is to use snakes or active shape models.

Energy minimisation Two types: Deformable models and Graph cuts The most recent segmentation methods are based on energy minimisation. Most current state-of-the-art techniques fall under this category. This is due to their flexibility and robustness [2]. This group encompasses two main subgroups: *deformable models* and *discrete combinatorial optimisation*.

The aim of deformable model techniques is to fit a deformable model, either a curve or a surface, to the image data. They may be formulated either explicitely, as a parametric contour (2D) or a surface, e.g. snakes [64] or active contours [65–67], or implicitly as a zero-level of a function with one dimension higher than that of the image data, e.g. as a level set [68]. This technique widely used in fluorescence image segmentation [69–74].

The aim discrete combinatorial optimisation is to search a finite countable solution space for the optimal solution. Optimality is defined with respect to some energy function, which embeds one or more criteria, which is to be minimised. The most common implementation exploits the graph cut framework. Graph cut segmentation has recently gained a lot of popularity and momentum in medical image segmentation (MIS) [75–82].

Other miscellaneous techniques Unsupervised clustering (k-means), Otsu binarization , dynamic programming , Voronoi diagrams , ellipse fitting, template matching, model matching, gradient flow tracking. The techniques presented are just a select few in a plethora segmentation techniques that have been used in microscopy image segmentation. A few other common techniques are unsupervised clustering segmentation using the k-means [83–85], Otsu binarization [86], dynamic programming [87, 88], Voronoi diagrams [89, 90], gradient flow tracking [91], etc. This is just a few more. Instead of cell segmentation converging to a robust, flexible and unified solution, the number of available options is steadily increasing [45]. There probably exists as many individual unique solutions for cell segmentation as there are problems.

2.5   Object Measurement and Analysis

What is the purpose of object analysis in FM? What is measured? The aim in fluorescence image analysis is to measure specific properties of interest which enable higher level decision making. Typically, these properties are quantitative measures. In this section we review some of the important quantitative measurements in digital image analysis. It is important to note that for some of the properties of interest, the accuracy of the measurements depend heavily on the accuracy on the segmentation. The properties of interest are application dependent, one might require just the object morphology of structure and hence properties like perimeter, area, shape, intensity, colour, etc are of significance. Alternatively, if one requires the colocalisation of cells, then distance discriminants, such as Euclidean distance, Manhattan distance, Chessboard distance, etc, are of significance [2, 92].

Object measures can be loosely classified into four catergories: geometric measures, histogram-based measures, intensity based measures and temporal measures. One can also argue a fifth catergory statistical classifiers although this is generally used in higher level analysis.

Size measures Perimeter, area and volume are common measures to describe the size of objects. Area and volume are suitable measures to describe the general size of an object. The perimeter of an object is distinctly useful in discriminating its shape complexity. Complex and irregular shapes need a larger perimeter to enclose its area.

Pose measures This measure is defines an objects location and orientation. The centroid is used as an objects' locale and its orientation is the measure of the angle subtended by its major axis.

Shape measures Shape features are used to distinguish objects from one another. These measures are generally translationally, rotationally and scale invariant and can be used independent of, or in conjunction with, the size measures. Commonly assessed shape parameters are thinness ratio to describe the regularity of an object, rectangularity, circularity, Euler number, moments, central moments, object dispersion, rotationally invariant moments, Zernike moments and elongation.

Shape descriptors Shapes descriptors provide a more wholesome way of decribing an object's shape than compared to the single parameter shape measures. Differential chain codes, and its two most common descriptors boundary chain code (BCC) and differential chain code (DCC), are used to represent the distance around an object. Fourier descriptors is another object distance measure that exploits the periodicity of BCC. There are also graph respresentations of which the two most common are minimum spanning tree (MST) [93, 94] and Delaunay triagulation (DT) [95, 96].

Distance measures There are many ways to compute the separation between objects. The most commonly assessed distance measures are Euclidean distance, Manhattan distance (also known as the City-block distance or absolute value metric), which is a more computationally efficient approximation of Euclidean distance, and the Chessboard distance (also known as the maximum value metric) [97, 98].

Intensity measures Images are segmented generally into region with low intra-region intensity distribution and high inter-region intensity distribution [56, 99]. Common intensity measures are integrated optical density (IOD) [100, 101], is simply the sum of all the gray levels that compose the object, its a reflection of the object's "mass" or "weight", average optical density (AOD), is the IOD divided by the objects area, and contrast.

Histogram measures These measure provide a measure of an object's intensity distribution. Common histogram-based measures are mean, standard deviation, skew, entropy and energy [102, 103].

Texture measures In image analysis texture refers to the spatial arrangement of gray level values [104] and hence a texture feature quantifies some characteristic of the intensity variation within an object. Common texture measures are statistical texture measures, gray-level co-occurrence matrix (GLCM) [105, 106] and power spectrum features [107, 108].

Ratiometric measures Some fluorescent dye respond to the changes in Calcium and Hydrogen ion concentration by changing its spectral properties of the fluorescent emission bands. In this case, a ratio of the intensity can be used to calculate concentration of calcium of pH value [11].

Temporal measures Considering the time domain, many interesting properties can be observed. Commonly computed properties of interest are motility [109–111], like velocity and acceleration, rate of growth, rate of change of colour, etc.

These measures are used in higher decision making processes such as the evaluation of a hypothesis to detect the presence of a certain disease. They are also used to aid in the understanding of biological mechanisms, events and interatctions [2].

Chapter 3

Mathematical Background

Optimisation approach in vision, "machinery/mechanics", literature review, ill-posed inverse problems.

Image segmentation falls under the mathemtical classification as being an *ill-posed inverse problem* [112, 113]. It is an inverse problem since we require a model from the observation, this simply means given the results, what are the causes. In image segmentation this translates to, given a 2D matrix of intensity values, which pixels belong to the object and which belong to the background. Image segmentation is also an ill-posed problem since their is a lack of uniqueness or stability of a solution [114], which are two of the three requirements for a solution to be *well-posed*, the other being existence. Image segmentation is an ill-posed because immense amount of information is suppressed in the acquisition processed [115–117]. Many tasks in vision are inherently or can be reformulated as ill-posed inverse problems e.g. scene reconstruction, stereo matching, image restoration, image deconvolution, etc. Computer vision is used heavily in industry, medicine and life science fields included, hence there is a need for robust, enviromentally resistant approach. The *optimisation approach* is an elegant way to obtain a solution. In computer vision, a problem can be posed as an optimisation problem as follows: We are given a coarse, discrete and noisy, approximation of the visual data, d, we aim to infer some hidden quantities x, labels, depth, probable pixel intensty, etc, based on it. We then have to design an *objective function*, also known as an *energy function* or *cost function*,

$$E : (x, d) \rightarrow \Re, \tag{3.1}$$

which has to be optimised such that the optimsation of the function provides a solution to the problem. $E(x, d)$ assigns an energy or a cost to each combination (x, d) of the input and hidden quantities. E provides a measure of goodness to how well the candidate solution x fits the expectation given the data d. In optimisation of this function we seek a minimum energy,

$$x^* = \arg\min_x E(x, d), \tag{3.2}$$

which has roots in Statistical Physics where lower energies correspond to more stable solutions. This gives us a general idea of how we should assign energies to solutions; better a solution, the lower an energy we should assign to it. In this case, a huge number of inference problems in vision can be solved by minimising the associated energy. A solution is only as good as the energy model and the optimisation technique. Once a precice energy and minimising algorithm are found, the problem is essentially solved [118].

Early attempts in computer vision would solve problems like these using iteration or relaxation methods [119, 120]. In these attempts the problems are solved in a Calculus of variations framework, this is still a popular approach to optimisation in vision since Poggio *et al.*. [112] proposed an integrated framework to regularisation theory for vision [121]. Many important

advancements in computer vision are proposals for a better energy, a better algorithm or both [118, 122–125]. In this thesis we focus on discrete energy optimisation using graph cuts for image segmentation.

Plan for the chapter. Image segmentation falls under a broader catergory of problems known as *labelling problems*. The aim is to find the best label, foregound/object or background, for each pixel. In Section 3.1 we briefly discuss labelling problems and its formulation as an energy minimisation problem.

3.1   Labelling Problems

Among the many computer vision problems, image segmentation is the most easy to understand labelling problem. A labelling problem is simply assigning, to an observation, a label that most accurately explains it. An observation can be anything that we wish to classify e.g. pixels, features, salient points, depth measurement, etc. A label is a description of that observation. There are two types of labels: *semantic labelling* (person, car, tree, sky, face, eye, etc) or *pixel-wise labelling* (texture, shape, colour, background/object, etc) [118, 126].

To formulate a labelling problem we need a set of *cites*, intuitively known as observations, and a set of *labels*, a set of explanations. The goal is to find the best explanation given the observations. In computer vision, the observations, can be features, image segments, etc. However, they will typically represent pixels in an image with some natual structure or ordering. Let

$$\mathcal{P} = \{1, 2, \ldots, n\}$$

be the set of n cites and

$$\mathcal{L} = \{l_1, l_2, \ldots, l_k\}$$

be the set of k labels. A discrete labelling is a map $f : \mathcal{P} \to \mathcal{L}$ that assigns each discrete variable f_p one value from $\mathcal{L}$ and $f = \{f_p\}_{p \in \mathcal{P}}$ which is known as a *configuration*. We are interested in binary segmentation, also known as *binarization*, which implies we have two explanations in our label set, $k = 2$. The labels of interest are the *background* and the *object*. Although the solution space is finite, it is very large and grows exponentially as the image size increases or as the number of labels increases. The number of possible configurations is given by $|\mathcal{L}|^{|\mathcal{P}|}$. Table 3.1 shows the largeness of the solution space even for very small images and a few labels. In pratice, the image sizes used in Table 3.1 is too small, hence finding a solution is not easy. Most often, settling for an approximate solution is "good enough".

TABLE 3.1: The impact of the number of cites and labels on the solution space

Image ($\mathcal{P}$)	Number of cites ($|\mathcal{P}|$)	Number of labes ($|\mathcal{L}|$)	Number of configurations $|\mathcal{L}|^{|\mathcal{P}|}$
64×64	$2^{12} = 4096$	2	$2^{2^{12}} = 2^{4096} = n$
128×128	$2^{14} = 16384$	2	$2^{2^{14}} = 2^{16384} = n^4$
64×64	$2^{12} = 4096$	3	$3^{2^{12}} = 3^{4096} \approx n^{1.585}$

3.2 Maximum A Posteriori Estimation for Discrete Models

As previously mentioned, image segmentation is can be viewed as a labelling problem. The problem is the huge search space in which the solution exists, or possibly more than one. We need a metric that is able to appropriately weight a configuration f. *Random Fields* are able to provide a structured and yet flexible probabilistic framework for labelling problems. *Markov Random Fields* (MRFs) and *Conditional Random Fields* (CRFs) are mostly used in vision tasks. We focus on the discrete image representation provided by MRFs in which we can embed the properties of a desired segmentation solution. MRFs are pivotal in designing, weighting and structuring graphs, so we give a brief introduction into the concepts needed to understand the probabilistic make-up for graph cut image segmentation.

3.2.1 Markov Random Fields

A *random field* (RF) is a stochastic process where each random variable is indexed by a spatial variable [127, 128]. A random field model can be intuitively represented as an undirected graph $\mathcal{G}(\mathcal{V}_{RF}, \mathcal{E}_{RF})$ where $\mathcal{V}_{\mathcal{RF}} = \{1, \ldots, n\}$ is the set of sites which correspond to a random variable for each pixel in $\mathcal{P}$, $\mathcal{E}_{RF}$ is the set of undirected edges which links the random variables. In vision, random variables which correspond to neighbouring or nearby pixels are linked. These links model interdependency and in images, nearby pixels exhibit a high degree of spatial correlation (similarity) [129]. Common connectivity arrangements in 2D images are 4- and 8-connectivity. Similarly, higher dimensional data can be represented using graph. For 3D images, common connectivity arrangements are 6- and 26-connectivity. Connectedness is illustrated in Figure 3.1 for 4-connectivity for 2D image data and 6-connectivity for 3D image data. In this thesis we are concerned with 2D images only. Two sites, p and q, are neighbours if edge $(p, q) \bigcup (q, p) \in \mathcal{E}_{RF}$. The set of neighbours of p are denoted $\mathcal{N}_p$. The RF associated with $\mathcal{P}$ is denoted as $\mathbf{Y} = \{Y_p : p \in \mathcal{P}\}$, where each Y_p can be assigned one of k labels from $\mathcal{L}$. A 4-connected RF is illustrated in Figure 3.2. A *clique c* is a fully connected subgraph; it is defined as $\forall p, q \in c, p \in \mathcal{N}_q$ and $q \in \mathcal{N}_p$. In a clique, each site is connected to all other sites.

The joint event $\{Y_1 = y_1, \ldots, Y_n = y_n\}$ where $y_p \in \mathcal{L}$ in called a *realisation* or *configuration* for the random field $\mathbf{Y}$. For readability we simplify the joint event notation to $\mathbf{Y} = \mathbf{y}$ where $\mathbf{y} = \{y_p : p \in \mathcal{P}\}$. The image segmentation problem is now in the form of an inference problem where the image $\mathbf{x}$ is the observation of a hidden random field $\mathbf{Y}$ and the solution is given by the *maximum a posteriori* (MAP), i.e. the solution is given by

$$\mathbf{y}^* = \arg\max_{\mathbf{y} \in \mathcal{Y}} \Pr(\mathbf{y}|\mathbf{x}), \tag{3.3}$$

where $\mathcal{Y}$ denotes the set of all possible labellings. $\mathbf{Y}$ is said to be a *Markov random field* (MRF) if:

$$\Pr(\mathbf{Y} = y) > 0 \qquad \forall y \in \mathbf{Y}, \qquad (Positivity), \tag{3.4}$$

$$\Pr(Y_p = y_p | x_{\mathcal{P} \backslash \{p\}}) = \Pr(Y_p = y_p | y_{\mathcal{N}_p}) \qquad \forall p \in \mathcal{P}, \qquad (Markovianity), \tag{3.5}$$

The positivity property constrains all configurations to have non-zero probability and is needed to ensure that the joint probability can be uniquely determined by the local conditional probabilities [130]. The Markovinatity property states that a site is conditionally independant of all other sites given it's neighbours.

MRFs are on of the most popular probabilistic modelling tools and was introduced to the computer vision community by Geman and Geman [131] and Besag [132]. MRFs allow us to model local contextual constraints, such as spatial interactions between pixels. According to Baye's rule, the posterior probability relation is:

$$\Pr(\mathbf{y}|\mathbf{x}) \propto \Pr(\mathbf{x}|\mathbf{y})\Pr(\mathbf{y}), \tag{3.6}$$

$\Pr(\mathbf{x}|\mathbf{y})$ encapsulates the depenency ofthe labels on the observation, it is the likelihood of observing $\mathbf{x}$ given $\mathbf{y}$. $\Pr(\mathbf{y})$ is the probability of that specific labelling among all labellings $\mathcal{Y}$. The joint distribution can be specified as a *Gibbs Random Field* (GRF) [133, 134]:

$$\Pr(x|y) = \frac{1}{Z} \prod_{c \in \mathcal{C}} \exp(-\Psi_c(\mathbf{x}_c)), \tag{3.7}$$

where $\mathcal{C}$ is the set of cliques. 3.3(a) shows a simple MRF construction. This MRF contains cliques of order one and two, i.e. $\mathcal{C} = \{1, 2, \ldots, 9, \{1, 2\}, \{1, 4\}, \ldots, \{8, 9\}\}$. 3.3(b) shows a more densely connected MRF where there are cliques of order one, two and three, i.e. $\mathcal{C} = \{1, 2, \ldots, 9, \{1, 2\}, \{1, 4\}, \{1, 5\}, \ldots, \{5, 9\}, \{8, 9\}, \{1, 2, 5\}, \{2, 3, 5\}, \ldots, \{5, 6, 9\}\}$. However, cliques of orders higher than two are ignored for computational reasons. In Equation 3.7 the term $\Psi_c(\mathbf{x}_c)$ is known as a *potential function* for the clique c, where $\mathbf{x}_c = \{x_i, i \in c\}$. The constant Z is called the *partition function* and ensures that the sum of all probabilities is one. After expanding Equation 3.7 for a maximum clique order of two, the conditional distribution of a pairwise MRF is:

$$\Pr(x|y) = \frac{1}{Z} \prod_{i \in \mathcal{V}} \exp(-\Psi_i(x_i)) \prod_{(i,j) \in \mathcal{E}} \exp(-\Psi_{ij}(x_i, x_j)), \tag{3.8}$$

where $\mathcal{V} = \{1, 2, \ldots, n\}$ and $\mathcal{E}$ is the set of pairwise edges, Ψ_i is the unary potential function, for first order cliques, and Ψ_{ij} is the pairwise potential function, for second order cliques.

3.2.2 MAP-MRF Estimation as Energy Minimisation

The equivalence of MRFs and GRFs, proven by Hammersely-Clifford thereom, means that maximising Equation 3.3 is equivalent to minimising Equation 3.2 [135]:

$$\mathbf{y}^* = \arg\max_{\mathbf{y} \in \mathcal{Y}} \Pr(\mathbf{y}|\mathbf{x}) = \arg\min_{\mathbf{y} \in \mathcal{Y}} E(\mathbf{y}, \mathbf{x}); \tag{3.9}$$

the most probable labelling yields the lowest energy. Obtaining the optimal labelling from Equation 3.9 does not guarantee that the segmented output will be good. The design of a good energy function, that captures all constraints and priors, is not easy. However, optimisation is harder still.

From Equation 3.7, if we take the negative log we get:

$$-\log(\Pr(x|y)) = \log(Z) + \sum_{i \in \mathcal{V}} \Psi(x_i) + \sum_{(i,j) \in \mathcal{E}} \Psi_{i,j}(x_i, x_j), \tag{3.10}$$

the constant Z is not need as it does not affect the final labelling. In this form, the equation is a sum of potentials, i.e. a sum of energies. The first term encodes the data constraints, E_{data}, and the second term encodes the prior constraints, E_{prior}. In addition, there is a factor that
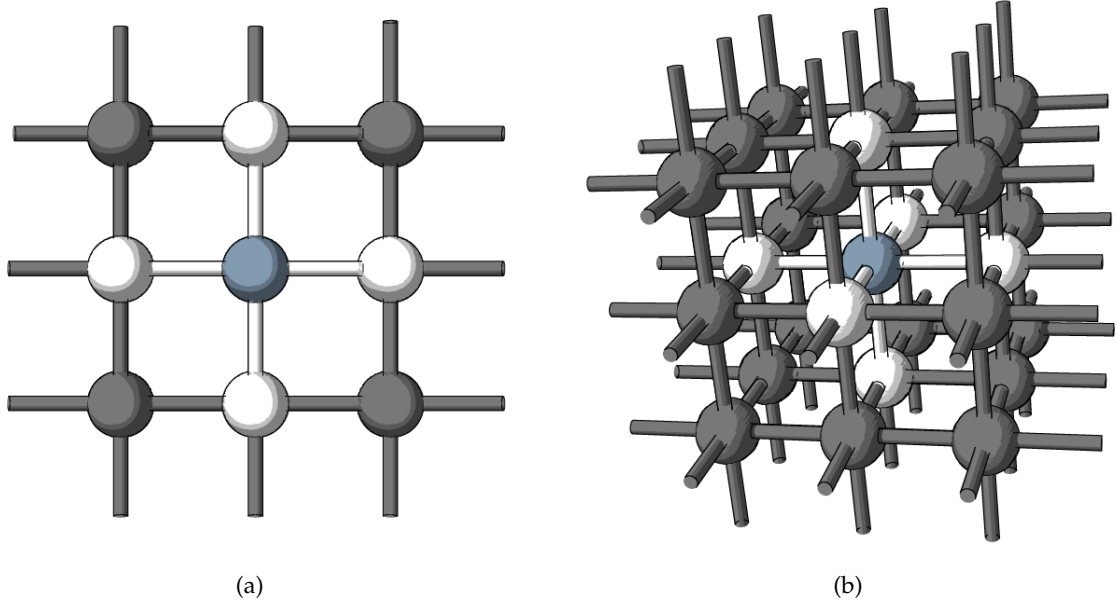
FIGURE 3.1: Common lattice structure for 2D and 3D image data. **(a)** Simplest connection of neighbouring pixels for 2D images. Each non-edge pixel is connected to 4 pixels. This is 4-connectedness. **(b)** Simplest connection of neighbouring voxels for 3D images. Each non-edge voxel is connected to 6 voxles. This is 6-connectedness.
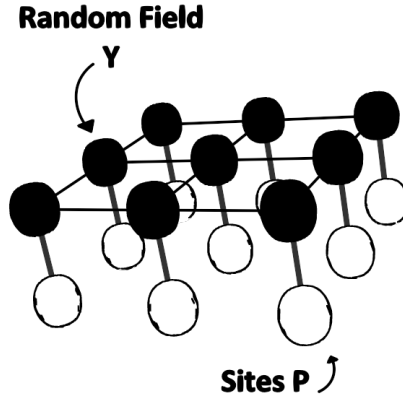
FIGURE 3.2: 4-connected random field $\mathbf{Y}$ over the sites $\mathcal{P}$.

controls the relative importance between the data and the prior, λ. The general form of the energy equation is:

$$E(f) = E_{data}(f) + \lambda E_{prior}(f), \tag{3.11}$$

where f is a particular labelling. The factor λ encodes our belief in the prior i.e. the larger λ is, the more we believe in the prior infomation. The data energy takes on the following form:

$$E_{data}(f) = \sum_{i \in \mathcal{V}} \Psi(x_i) = \sum_{p \in \mathcal{P}} D_p(f_p). \tag{3.12}$$
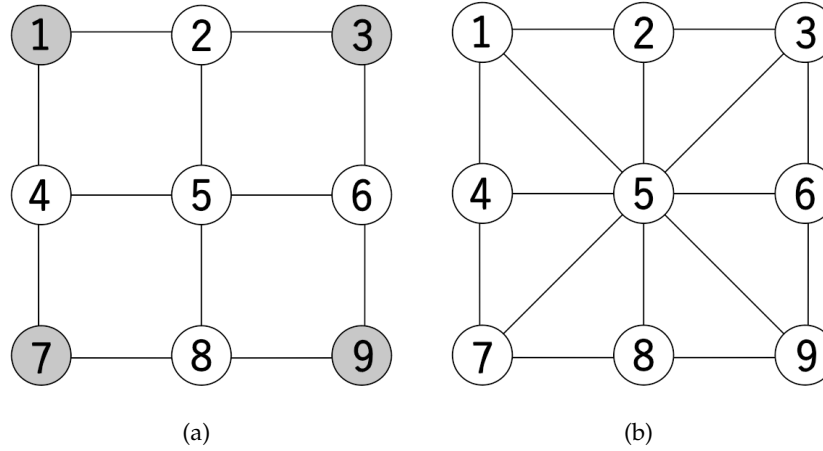
FIGURE 3.3: Caption. **(a)** Caption. **(b)** Caption.

D_p measures the level of agreement between the label f_p and the pixel p. A common approximation is to assume independency observations, and this makes designing D_p relatively straightforward. The only restriction is $D_p(f_p) \in \Re^+$. The prior energy takes on the following form:

$$E_{prior}(f) = \sum_{(i,j)\in\mathcal{E}} \Psi_{i,j}(x_i, x_j) = \sum_{\{p,q\}\in\mathcal{N}} V_{\{p,q\}}(f_p, f_q). \tag{3.13}$$

$V_{\{p,q\}}(f_p, f_q)$ is known as the *neighbourhood interaction function*. The aim of this function is to encourage neighbouring random variables to take on the same label, i.e. it penalises neighbouring pixels p and q if they have different labels. The form of $V_{\{p,q\}}(f_p, f_q)$ is application dependant and is more tricky to design. In image segmentation, the most common prior is that of smoothness, i.e intra-object pixel intensities are assumed to be the same or vary gradually within some range, it is at edges or boundaries where this assumption is violated. The general form in Equation 3.11 can be rewritten as:

$$E(f) = \sum_{p\in\mathcal{P}} D_p(f_p) + \lambda \sum_{\{p,q\}\in\mathcal{N}} V_{\{p,q\}}(f_p, f_q). \tag{3.14}$$

When we say MAP-MRF estimation we generally mean energy minimisation. Energy minimisation is a non-trivial task given the intractability of the search in the solution space. Energy minimisation can be catergorised into *global energy minimisation* and *local energy minimisation*. We briefly discuss some of the energy minimisation techniques.

Iterated Conditional Modes (ICM) This is a deterministic method that converges to a local minimum [136]. It a greedy technique that was introduced into vision by Besag [132, 137]. The algorithm iteratively chooses the label that results in the largest decrease in energy at each site until convergence. It is extremely sensitive to initialisation as the dimensionality of the space increases with non-convex energies.

Simulated Annealing This is a stochastic optimisation method that simulates the annealing of a material. It is one of the only general-purpose energy minimisation methods. It was devloped and published independantly by Černý [138] and Kirkpatrick *et al.* [139] and was

introduced into computer vision by Geman and Geman [131]. The algorithm is initialised with a random labelling. Each pixel is then visited and a local random change is made. If the change results in a lower energy then it is accepted, else the change is accepted based on a probability parameter, i.e. the temperature. With certain cooling schedules the global minimum can be obtained however, this is horrendously slow in practise so sub-optimal schedules are used instead [131].

Genetic Algorithms (GAs) GAs have been succesfully employed in energy minimisation for image segmentation [140–144]. GAs work by performing simultaneous local searches that optimise the energy function via a random walk in the search space. The algorithm terminates by choosing the search that found the lowest energy for the energy functional. Their drawback is their inability to guarantee a global optimum [145].

Gradient Descent Explicit differentiation under the Euler-Lagrange equations can be used to obtain a solution [145]. Each modified energy functional must be accompanied by derivation of obtaining a minimum [64, 65, 146, 147]. With an artificial time step, this algorithm deforms a shape, using the gradient descent process, which is equated to the set of Euler-Lagrange equations. When the deformable models come to rest the equations are satisified. There are two common drawbacks with this method: Firstly, image noise can severely hinder the gradient descent process and this could lead to instability of the deformation process. Secondly, increasing the number of dependant variables increases the complexity of the search space and time to converge to an optimal solution as there are more derivatives to calculate [145].

Loopy Belief Propagation (LBP) The belief propagation algorithm was initially designed to be used on acyclic graphs where it able to obtain a global minimum [148]. However, the same algorithm has been succesfully applied on cyclic graphs firstly for error-correcting code problems [149] and then later on in vision [150]. Convergence is not guaranteed as the algorithm might get stuck alternating between two labels [148].

Graph Cuts Graph cuts have become an indespensable tool in computer vision. For a restrictive class of energy functions, *submodular functions*, it is able to obtain a global minimum [151–154]. For non-submodular energy functions it is able to find approximate solutions with strong local optimality [122, 155–157]. Greig *et al.* was the first to use graph cuts in vision to find an exact solution to a certain energy function for the binary image restoration problem [158]. However, it did recieve much attention and remained buried for almost ten years primarily because of the disinterest in binary image restoration and that, at the time, it's optimisation was notoriously slow which made it an unappealing technique when compared to stochastic optimisation methods, like simulated annealing, which was popular at the time. In the last two decades graph cut optimisation has been a major focus as a key tool in optimisation since Roy and Cox [159] used it to solve more interesting problems in multi-camera stereo. Shortly after, Boykov *et al.* generalised the method for determining the MAP estimate of MRFs [160]. Graph cut optimisation is the technique of focus in this thesis.

3.3 Introduction to Graph Cuts

Graph cuts is a combinatorial optimisation method which can be used to minimise energies of the form presented in Equation 3.14. The aim of graph cuts is to partition a graph into mutual exclusive subgraphs by removing the edges whose sum of capacities is a minimum. We

are interested with cutting the graph into two subgraphs. Graph cut algorithms existed long
before their use was employed in vision, this is primarily due to the lack of computational
power available at the time. Fortunately, computational power is no more as rare a resource
as it was previously and this has paved a way into exploiting the power of graph data struc-
tures. As a result, this has also lead to vision-specific graph-cut algorithms. There are primar-
ily three types of graph-cut algorithms: *Augmenting Path Algorithms*, such as Ford-Fulkerson
algorithm [161], Dinic algorithm [162], Edmond-Karps algorithm [163] etc, *Preflow-Push Algo-
rithms*, also known as *Push-Relabel* [164], and *Move-Making Algorithms* such as the α-β Swap
[122], α-Expansion [122], etc.

3.3.1   Network Theory and the Min-cut Problem

In this section we briefly cover the foundation aspects to understanding graph cuts. We cover
Flow networks, a branch of Graph Theory also known as *Transportation networks*, and introduce
the *Min-cut problem*. For a solid understanding in Graph Theory and Flow Networks see [165–
168]. A brief introduction is given in Appendix A.

Network   A network $\mathbf{N} = (V, E)$ is a directed graph with a source node s, a sink node t and a
strictly positive capacity on every edge. That is, for each edge $e \in E$, the capacity, $c(.)$, obeys
$c(e) \in \Re^+$. The **source node** only has out-going edges, $d_{in}(s) = 0$ and $d_{out}(s) \geq 0$. The **sink
node** only has incoming edges, $d_{in} \geq 0$ and $d_{out} = 0$. An example of a network is illustrated in
Figure 3.4.
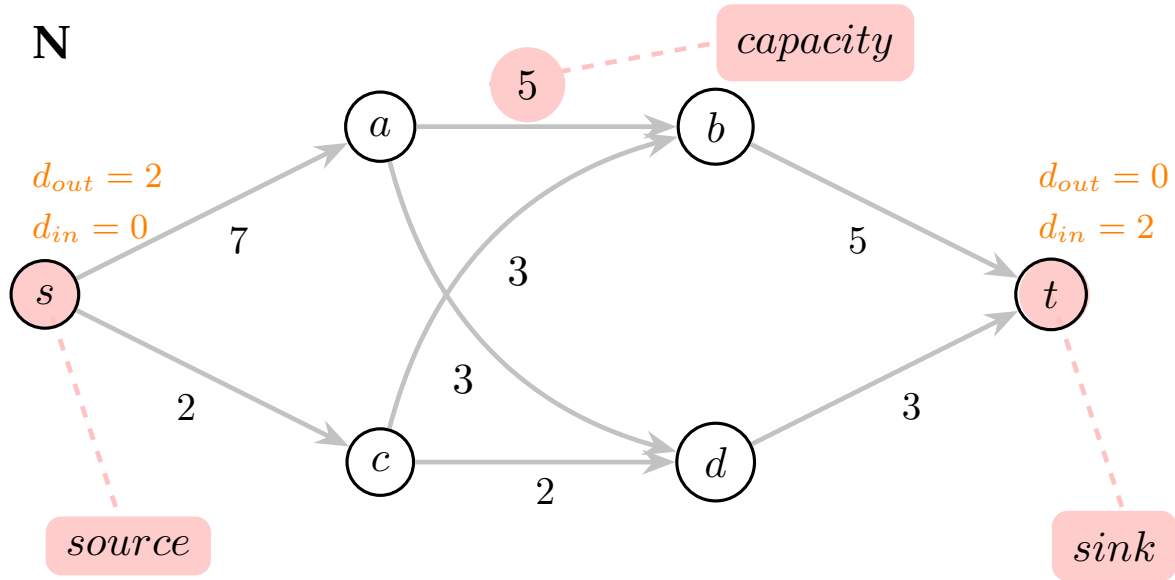
FIGURE 3.4: Network **N** with no flow. The in-degree and out-degree for the source, **s**, and the sink, **t**,
are shown next to the corresponding node.

Flow   A flow $f : V^2 \longrightarrow \Re^+$ is associated with each edge $e = (u, v)$ such that:

1. for each edge $e \in E$ we have $0 \leq f(e) \leq c(e)$. That is, the flow is positive and cannot
   excees the capacity of the edge.

2. for each intermediate node $v \in V \backslash \{s, t\}$ the in- and out-flow of that node $\sum_{u \in V^-(v)} f(u, v) = \sum_{u \in V^+(v)} f(v, u)$.

The **total flow** F of a network is then what leaves the source s or reaches the sink t:

$$F(\mathbf{N}) := \sum_{u \in V} f(s, u) - \sum_{u \in V} f(u, s) = \sum_{u \in V} f(u, t) - \sum_{u \in V} f(t, u) \tag{3.15}$$

An example of a network with non-zero flow is illustrated in Figure 3.5.
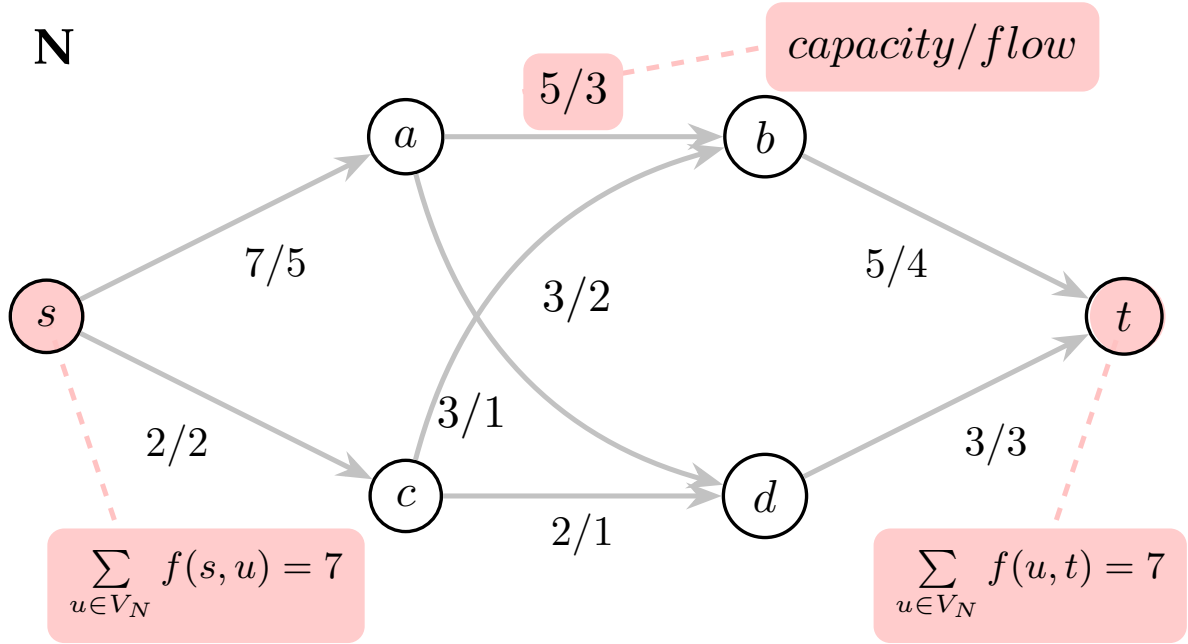
FIGURE 3.5: Network **N** with flow. The flow out of the source node, **s**, is equal to the flow into the sink node, **t**. For all other nodes, the flow-in is equal to the flow-out. This is the conservation of flow principle. This is only part of the network. The remaining part is the residual graph which shows the amount of reverse flow is available on an edge.

Cut A cut of a network $\mathbf{N} = (V, E)$ is a partitioning of the vertex set $V = P \bigcup \bar{P}$ into two disjoint sets P containining the source node s and $\bar{P}$ containing the sink node t. $P \bigcap \bar{P} = \emptyset$. The **cost** of a cut is the sum of the capacity of the edges $(u, v) \in V$ where $u \in P$ and $v \in \bar{P}$:

$$\kappa(P, \bar{P}) = \sum_{u \in P; v \in \bar{P}} c(u, v) \tag{3.16}$$

A network with a valid cut is illustrated in Figure 3.6. Invalid cuts are shown for the same network in Figure 3.7 and Figure 3.8.

Maximal Flow The largest amount of flow that is able to reach the sink from the source is known as the maximal flow. A network with a maximal flow, also known as a *max-flow*, is illustrated in Figure 3.9.

$$S = \{s, a\}, \ \ T = \{t, b, c, d\}, \ C = \{(sc), (ab), (ad)\}$$
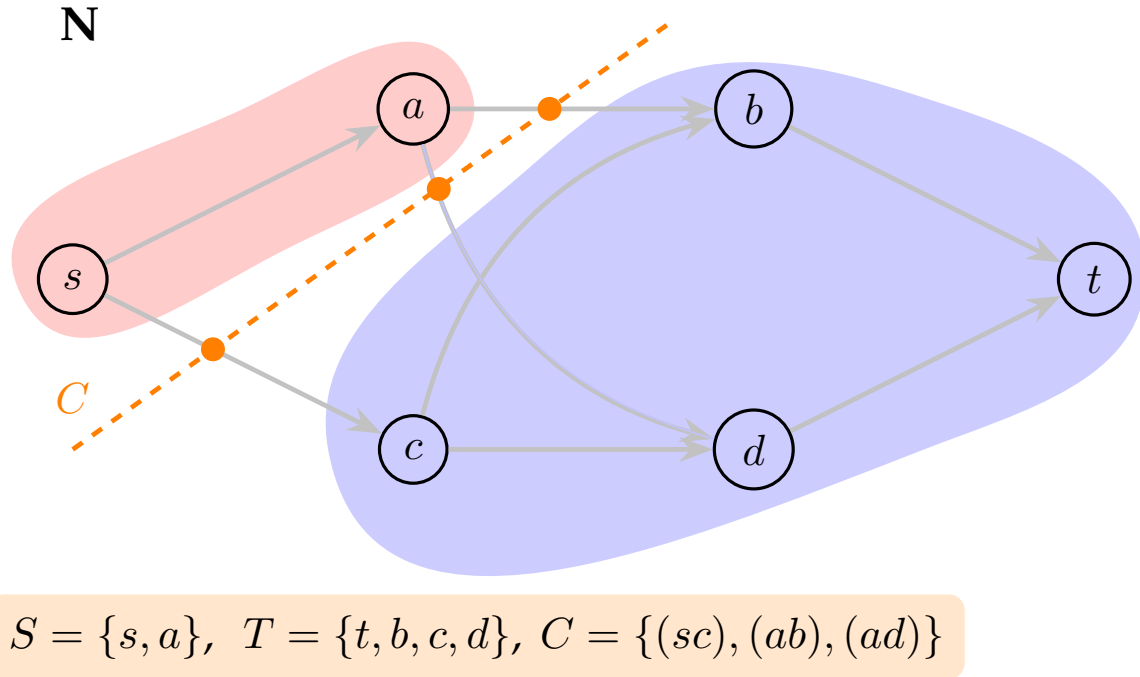
FIGURE 3.6: Network **N** with with a valid cut **C**. The nodes within the red region are reachable from the source and the nodes within the blue region are able to reach the sink. The cut set, **C**, is show in the orange filled block.
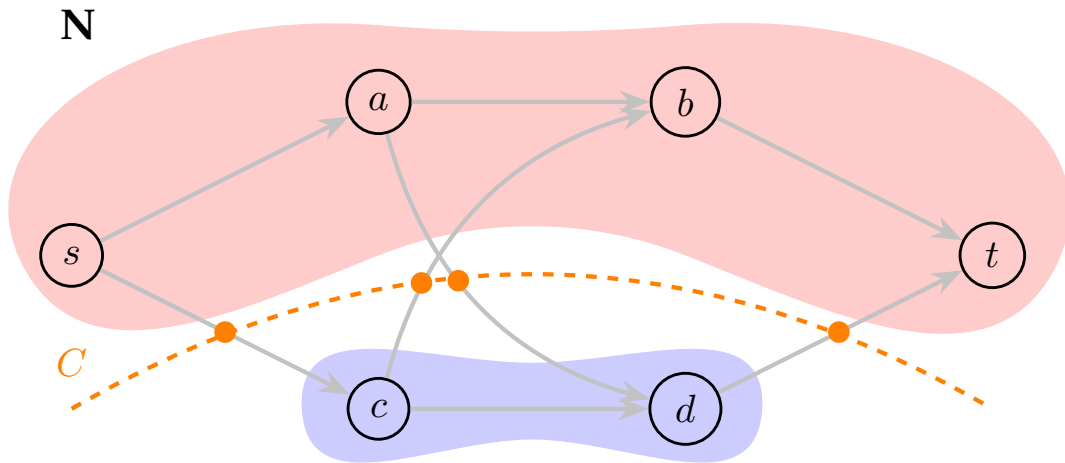
FIGURE 3.7: Network **N** with with a invalid cut **C**. The cut does not partition source node **s** and sink node **t** into distinct sets.

Minimal Cut A cut C on a network $\mathbf{N} = (V, E)$ is a minimal cut if there exists no other cut C' where $\kappa(C') < \kappa(C)$. A network with a minimal cut, also known as a *min-cut*, is illustrated in Figure 3.10.

Talk about the max-flow/min-cut duality, non-uniqueness. In Figure 3.9 and Figure 3.10 the maximum flow and the minimum cut yield the same answer. This is not a coincidence, in fact the two problems are duals of each other, known as the *max-flow min-cut duality*. This

N
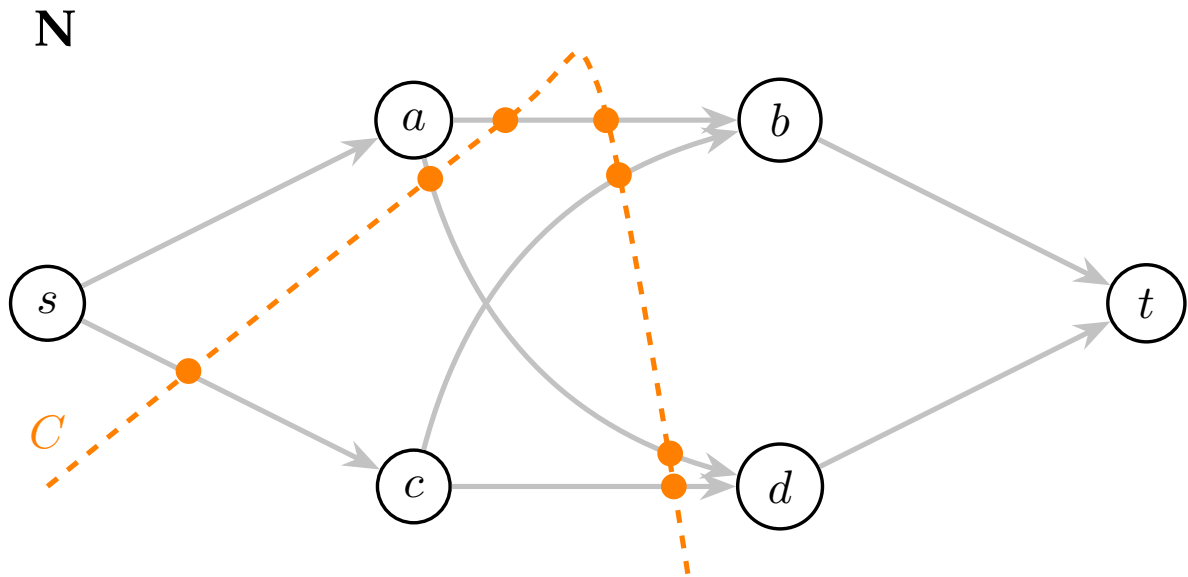
FIGURE 3.8: Network **N** with with a invalid cut **C**. The cut partition partitions the graph into more than two sets and the cut intersects the edges *ab* and *ad* twice.

N
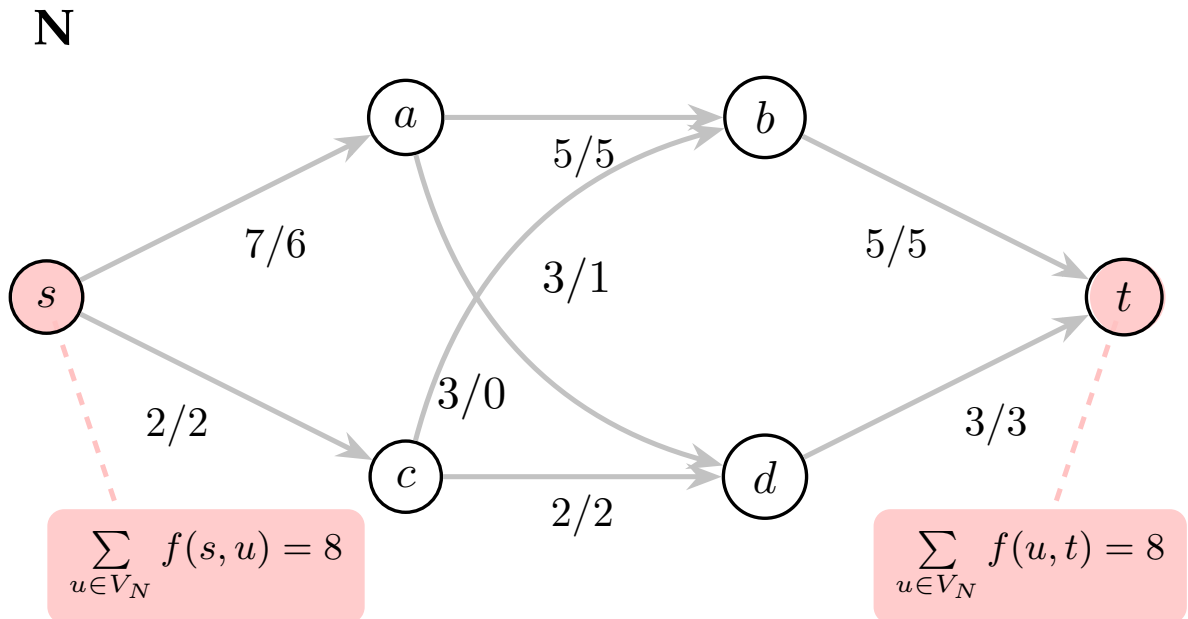
FIGURE 3.9: Network **N** with maximum flow. There is no way to push more flow out of the source into the sink without breaking the rules for the conservation of flow.

was proven by P. Elias, A. Feinstein, and C.E. Shannon [169] and by Ford and Fulkerson [161] independently in 1956. This duality is immensely helpful in developing machine algorithms to compute the minimum, since it is easier to find a maximum flow. It is important to realise that there maybe many cuts that can be minimum cut and many flow configurations that can yield the maximum flow, hence the solution is not guaranteed to be unique only an optimum.
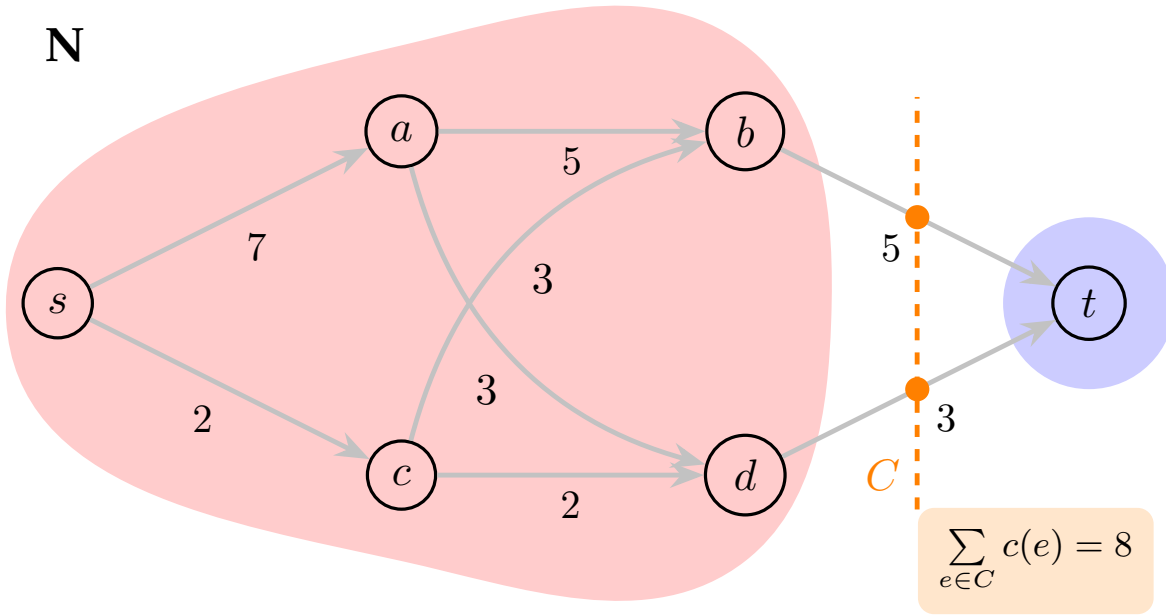
FIGURE 3.10: Network **N** with minimal cut **C**. The sum of the capacity of all the edges in the cut set is the minimum of all possible valid cuts on the network **N**.

3.3.2   Image Segmentation Graph Structure

Graph construction. Special terminology: n-links, t-links, etc. Undirected to directed conversion. Labels as terminals. Construction with and witthout seeds. Edge weighting -> leave submodular functions to their own section. In graph cut image segmentation the energy function, defined by the image, has to be represented as a graph, specifically a network. We now look at how to 2D binary segmentation energy is constructed as a graph. The graph that is constructed uses the MRF, Section 3.2.1, model of the image as its base. Each pixel is a node in the graph. The connections between "pixel nodes" are bi-directional, which is generally decomposed into two uni-directional edges, and are known as *n-links* which is synonymous with *neighbour-links*. Additionally, each label is also represented as a node. Each "pixel node" is attached to all "label nodes". In binary, segmentation, there are two labels i.e. object and background. The edges that connect "label nodes" to "pixel nodes" are called *t-links* which is synonymous with *terminal-links*. In keeping with network construction, one label will be the source and the other will be the sink. The t-link weights are generally learned from user input seeds or automatically generated seeds. Seeds mark which type of pixels belong to the object and which belong to the background, an illustration is shown in Figure 3.11(a). With the seed data and the neighbourhood interaction, we can construct a graph representation of the energy to be minimised over the image as illustrated in Figure 3.11(b). Once a graph has been constructed, we then call upon a max-flow/min-cut method which will minimise the energy function by partitioning the graph into two subgraphs, as shown in Figure 3.11(c). All pixels are classified according to which "label node" they're still attached to after the max-flow/min-cut algorithm has run, this is illustrated in Figure 3.11(d).
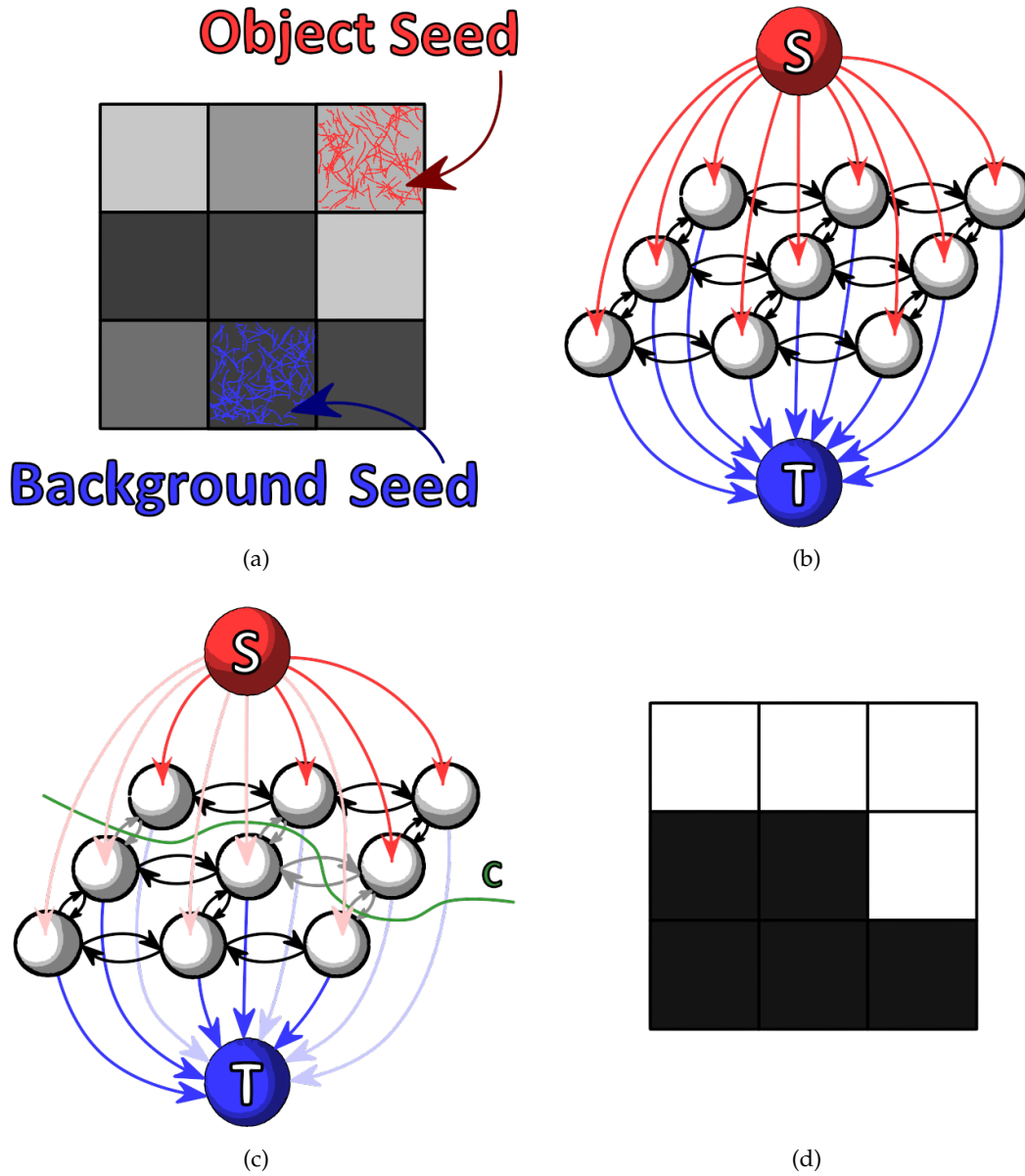
FIGURE 3.11: Overall process of the graph cut image segmentation process. **(a)** Image with object and background seeds. **(b)** Graph representation of the energy function to be minimised over the image. The n-links are represented by black arrows, the t-links from the source are shown in red, and the t-links to the sink are shown in blue. **(c)** Minimised energy function by cut C. The light red, light blue and grey edges are those that belong to the cut set C. **(d)** Segmentation mask after label assignment. In this case, all nodes that are still attached to the source, their corresponding pixel label is shown in white, similarly, nodes that are connected to the sink have their corresponding pixel labels shown in black.

3.3.3 Submodular Functions

In the previous section we talked about representing the energy function as a graph. However, not all energy functions can be represented as a graph. Moreover, minimising an arbitrary energy function, even if the energy is binary, is NP-hard [170]. There does exist a class of functions which is graph representable and is able to be minimised in polynomial time, i.e.

an exact global minimum can be obtained in a single graph cut. These energy functions are known as *submodular functions*. They are sometimes referred to as "discrete analog of convex functions" since they're the easiest to minimise, much like convex functions. For an energy to be submodular, it must satisfy the submodularity constraint:

$$f^p(a, b) + f^p(a+1, b+1) \le f^p(a, b+l) + f^p(a+1, b), \qquad \forall a, b \in \mathcal{L}, \tag{3.17}$$

where $\mathcal{L}$ is an ordered label set. The type of energies we are concerned with are second order binary energies, and enforcing the submodularity constraint means that the energy function must to satisfy:

$$E_{ij}(0, 0) + E_{ij}(1, 1) \le E_{ij}(0, 1) + E_{ij}(1, 0), \qquad \forall \{i, j\} \in \mathcal{N}, \tag{3.18}$$

where $\mathcal{L} = \{0, 1\}$. It is necessary and sufficient for an energy function to satisfy Equation (3.18) to compute the exact global minimum in polynomial time in a single graph cut. This was first characterised by Kolomogorov and Zabih [151].

3.4   Graph Cut Algorithms for Energy Minimisation

Image segmentation via graph cuts can be seen as three main stages. Firstly the problem is modelled and a suitable energy function is designed. Generally, this is a trade-off between accuracy and constraining to the submodularity constraint. Secondly, a graph is constructed which represents the energy function. Thirdly, and finally, the energy function is minimised by using a max-flow/min-cut algorithm. In this section we discuss the last stage. The minimisation algorithms are either general or specific to the energy functions. We briefly discuss some of the most common max-flow algorithms.

3.4.1   Ford-Fulkerson

The Ford-Fulkerson max-flow algorithm [161] is designed to on an arbitrary network with one source and one sink. Ford and Fulkerson proved that the max-flow and min-cut problems are duals of each other, hence solving one means that you've obtained the solution to the other. Augmenting path algorithms iteratively search for open path from the source to the sink. When a path is found, the maximum flow that can be pushed in that path is pushed through that path by incrementing the flow on each edge of that path. The path is said to be *augmented*. If there are no available paths which can be augmented, the solution has been found and the algorithm terminates. The maximum flow is then obtained by the flow leaving the source or the flow entering the sink. A Ford-Fulkerson max-flow algorithm is shown in Algorithm 1. The min-cut, and segmentation, problem can be solved using Algorithm 2. In image segementation we only require the sets $\mathcal{V}_S$ and $\mathcal{V}_T$, so the last step is not necessary. The Ford-Fulkerson algorithm exhibit very poor performance. The primary cause is that each new augmenting path has to be found from scratch. In [153], they countered this by reusing as much information as possible from the existing path. Running time, complexity, properties for network flow, etc of Ford-Fulkerson.

Algorithm 1 Ford-Fulkerson Max-flow

1: **procedure** MAXFLOW(G) ▷ The maximum flow on graph G
2:    **while** $p = findPath(s, t)$ **do** ▷ Find an open path p between s and t
3:        **if** $p = \emptyset$ **then** ▷ See if a solution has been found
4:            break
5:        **end if**

6:        $maxflow_p = 0$
7:        **for each** edge $e \in p$ **do** ▷ Find max-flow on path p
8:            $maxflow_p \leftarrow min(maxflow_p, c(e) - f(e))$ ▷ Residual capacity on edge e
9:        **end for**

10:        **for each** $e \in p$ **do** ▷ Push max-flow on path p
11:            $f(e) \leftarrow f(e) + maxflow_p$ ▷ Augment each path on path p with flow $maxflow_p$
12:        **end for**
13:    **end while**
14: **end procedure**

Algorithm 2 Min-cut from Max-flow

1: Calculate max-flow on $\mathcal{G}$
2: Partition $\mathcal{V}$ into $\mathcal{V}_S$ and $\mathcal{V}_T$
3: $\mathcal{C} = \{(u, v) \in \mathcal{E} | u \in \mathcal{V}_s \wedge v \in \mathcal{V}_T\}$

3.4.2 Dinic/Edmonds-Karp

The Ford-Fulkerson max-flow algorithm is a very inefficient method to finding the max-flow. In practice the runtime is too high making it unfavourable. An improvement on this augmenting path based algorithm was designed by Dinic[162] in 1970 and independently by Edmonds and Karp[163] in 1972. The improvement is a change in searching for a path which can be augmented. The Edmonds-Karp algorithm finds the shortest path from the source to the sink by defining the lenght of all edges to be one and using a breadth first search form the source. The amount of flow to be augmented into each path is the minimal residual capacity of the edges in the path. This ensure that on each augmentation atleast one path is *saturated*. The edges that become saturated are said to be *critical*. The Edmonds-Karp max-flow algorithm is shown in Algorithm 3. The worst-case complexity is $O(|\mathcal{V}|, |\mathcal{E}|^2)$. Depending on the graph structure other searching strategies may be more efficient, eg. depth first search (DFS) [171], etc.

3.4.3 Push-Relabel

Originally developed by Andrew V. Goldberg and Robert E. Tarjan [164]. Previous algorithms, such as Ford-Fulkerson, used the concept of residual networks and augmenting paths to determine max-flow. Push-Relabel used the concept of preflow to determine max-flow instead of augmenting paths. Sometimes referred as the *Preflow-Push Algorithm*. Preflow is a concept originally developed by A.V. Karzanov.

Algorithm 3 Edmonds-Karp Max-flow

1: **procedure** MAXFLOW(G)   ▷ The maximum flow on graph G
2:     **while** $p = BFS(s, t)$ **do**   ▷ Find the shortest and open path p between s and t
3:         **if** $length(p) = 0$ **then**   ▷ See if a solution has been found
4:             **break**
5:         **end if**

6:         $minrescap_p = \infty$
7:         **for each** edge $e \in p$ **do**   ▷ Find augmenting flow to saturate an edge
8:             $minrescap_p \leftarrow min(minrescap_p, c(e) - f(e))$ ▷ Residual capacity on edge e
9:         **end for**

10:         **for each** $e \in p$ **do**   ▷ Push flow on path p
11:             $f(e) \leftarrow f(e) + minrescap_p$ ▷ Augment each edge with flow $minrescap_p$
12:         **end for**
13:     **end while**
14: **end procedure**

The algorithm works at converting a preflow, f, into a normal flow and then terminates. This flow also turns out to be the maximum flow. Goldberg and Tarjan defined a generic Push-Relabel algorithm which solves the maximum flow problem.

Preflow A preflow is a real-valued function, f, on vertice pairs. The total flow into a vertex can exceed the flow out of a vertex but not vice versa.

A preflow where all $v \in V - \{s, t\}$ has a flow excess of zero, $e_f(v) = 0$, is a normal flow. The preflow function is also referred to as the **s-t preflow**.

Preflow must satisfy:

1. Capacity Constraint
   $\forall u, v \in V, f(u, v) \leq c(u, v)$

2. Antisymmetry/Skew Symmetry
   $\forall u, v, \in V, f(u, v) = -f(v, u)$

3. Nonnegative Constrain
   The flow into $v \in V - \{s\}$ must be greater than or equal to the flow out of v. $\forall u \in V, v \in V - \{s\}, \sum f(u, v) > 0$

Flow Excess Flow excess, $e_f(v)$, is the net flow into v where $v \in V$ for some preflow f.

$$e_f(v) = \begin{cases} \infty & \text{if } v = s \\ \sum_{u \in V} f(u, v) & \text{if } v \in V - \{s\} \end{cases}$$

Active Vertex An active vertex/node is a vertex v which satisfies all of the properties:

1. Not a source or sink, $v \in V - \{s, t\}$

2. Positive flow excess, $e_f(v) > 0$

3. Has a valid label, $d(v) < \infty$

Push-Relabel also uses the concept of a residual graph, $G_f^* = (V, E_f)$.

Residual Capacity The residual capacity of a preflow is defined as $r_f(v, w) = c(v, w) - f(v, w)$.

Residual Edges The residual edges for a preflow f is defined as the set of edges with positive residual capacity. $E_f = \{(v, w)\}|r - f(v, w) > 0$.

Labelling Push-Relabel also use a valid labelling function, d, to determine which vertex pairs should be selected for the push operation.

A valid labelling , d, is a nonnegative integer function applied to all vertices to denote a label. The labelling is often referred as the height or distance from the sink node, t. This function is sometimes compared to the physical intuition that liquids naturally flow downhill.

A valid labelling for a preflow consists of:

1. For $v \in V, 0 \le d(v) \le \infty$

2. $d(s) = |V|$ (source condition)

3. $d(t) = 0$ (sink condition)

4. $d(v) = d(w) + 1$ for every residual edge $(v, u) \in E_f$

A labelling d and a preflow f are said to be compatible id d adheres to the properties above.

The algorithm pushes flow excess starting at the source, s, along all vertices towards the sink, t. The algorithm maintains a compatible vertex labelling function, d, to the preflow, f. The labelling is usedto determine where to puch the flow excess. The algorithm repeatedly performs either a push or a relabel operation so long as there is an active vertex in G_f^*.

Push Operation The push operation is used to move flow from one vertex to another. The transfer of excess can be performed across the vertex pair $(v, w) \in E_f$ if:

1. v is an active vertex

2. the edge has positive residual capacity, $r_f(v, w) > 0$

3. the label distance $d(v) = d(w) + 1$

This allows the algorithm to move δ excess flow: $\delta = min(e_f(v), r_f(v, w))$ from v to w. A push is considered *saturating* if no more flow can be sent over the edge, $\delta = r_f(v, w)$. A push is considered to be *non-saturating* if all the excess from v the push over the edge and the edge still has some capacity, $\delta = e_f(v)$. The push operation is shown in Algorithm 4.

Relabel Operation The relabel operation is used to increase the label value of a single active vertex so that excess flow can be pushed out of the active vertex. The relabel operation is performed when all the residual edges of the active vertex have positive residual capacity, $r_f(v, w) > 0$. This implies that v's label is less than or equal to all vertices, $d(v) \le d(w)$, meaning that no push operation across the edges is possible given the push condition $d(v) = d(w) + 1$.

The relabel operation for some vertex v selects the smallest label for the vertices with positive residual edges, $r_f(v, w) > 0$. The active vertex is then assigned the smallest label value $+1$ such that $d(v) := min\{d(v) + 1|(v, w) \in E_f\}$. This will alow the vertex v to potentially push its excess flow to atleast one of the othe vertices during the algorithm's next iteration. The relabel operation is shown in Algorithm 5.

Algorithm 4 Push Operation

Input: Preflow f, labels d, and (v, w) where $v, w \in V$
Output: Preflow f
Applicable: if $v \in V - \{s, t\}$, $d(v) < \infty$, $e_f(v) > 0$, $r_f(v, w) > 0$ and $d(v) = d(w) + 1$

  1: **procedure** PUSH(G, G^*, v, w)
  2:     $\delta \leftarrow min(e_f(v), r_f(v, w))$ ▷ Find the maximum flow can be pushed from v
  3:     $f_G(v, w) \leftarrow f(v, w) + \delta$ ▷ Push flow and update residual graph
  4:     $f_{G^*}(w, v) \leftarrow f(w, v) - \delta$
  5:     $e_G(v) \leftarrow e_f(v) - \delta$ ▷ Update excess on G and its residual graph G^*
  6:     $e_{G^*}(w) \leftarrow e_f(w) + \delta$
  7:     **return** δ
  8: **end procedure**

Algorithm 5 Relabel Operation

Input: Preflow f, labels d, and $v \in V - \{s, t\}$
Output: Labels d
Applicable: if $v \in V - \{s, t\}$, $d(v) < \infty$, $e_f(v) > 0$, and $\forall w \in V, r_f(v, w) > 0$ which implies $d(v) \leq d(w)$

  1: **procedure** RELABEL(v)
  2:     $d(v) \leftarrow \infty$
  3:     **for each** vertex $w \in \mathcal{N}_v$ **do**   ▷ Consider all the nighbours of v
  4:        **if** $\{(v, w) \in E_f\} \neq 0$ **then**   ▷ Is w reachable from v
  5:           $d(v) \leftarrow min(d(v), d(w) + 1)$
  6:        **end if**
  7:     **end for**
  8:     **return** d
  9: **end procedure**

Discharge Operation The coordination of pushing excess flow from and relabelling a vertex is handled in a discharge operation. The idea is to push as much excess flow, from the currently picked active vertex, to its neighbours. If no more flow can be pushed but the node is still active then relabel it. The discharge operation is shown in Algorithm 6.

The algorithm also maintains a list of active nodes to dischage. The complete Push-Relabel algorithm is shown in Algorithm 7. The algorithm repeatedly pushes flow between nodes until their are no more active nodes. Worst-case Complexity, etc.

There are many variations of the push-relabel algorithm [164, 172]. Most of these are heuristic implementations to reduce execution time. One such heuristic is the *First-in First-out* (FIFO) [164]. With this implementation the theoretical run-time is shown to be $O(|\mathcal{V}|^3)$. Cubic complexities are unaccpetable in practice, however in practice this heuristic displays a great boost in speed optimisation. Emperical runtime over theoretical runtime is accepted in practice.

Instead of discharging nodes in the order that they entered the *Active_node* list, a better heuristic is to dishparge nodes in descending order of node level/height. This heurustic is known as *Highest level first* (HLF). Flow is pushed from higher level nodes to lower level nodes first. This allows a greater dissipation of flow.

Algorithm 6 Discharge Operation

Input: $v \in V - \{s, t\}$
Output: State of node
Applicable: if $v \in V - \{s, t\}$, $d(v) < \infty$, $e_f(v) > 0$

1: **procedure** DISCHARGE(v)
2:     $i \leftarrow v.current\_neighbour$ ▷ index of the current neighbour under consideration
3:     **while** $(e(v) > 0) \wedge (i < \text{size}(v.neighbour))$ **do**   ▷ *neighbour* is the list of neighbours
4:         **if** $(d(v) == d(v.neighbour[i]) + 1) \wedge (r_f(v, v.neighbour[i]) > 0)$ **then**
5:             push(v,$v.neighbour[i]$)
6:             $i \leftarrow (i + 1)$
7:         **end if**
8:         **if** $e(v) > 0$ **then**
9:             relabel(v)
10:         **end if**
11:         $v.current\_neighbour \leftarrow i$ ▷ Pick up from this neighbour on the next discharge
12:         **return** $e(v) > 0$ ▷ Is node still active
13:     **end while**
14: **end procedure**

Algorithm 7 Push-Relabel Maxflow Algorithm

Input: $\mathcal{G} = (\mathcal{V}, \mathcal{E})$
Output: Maximum flow, f

1: **procedure** MAXFLOW($\mathcal{G}$)
2:     $d(s) \leftarrow |\mathcal{V}|$ ▷ Initilise the height of all nodes
3:     $d(t) \leftarrow 0$
4:     **for** $\forall v \in \mathcal{V} - \{s, t\}$ **do**
5:         $d(v) \leftarrow 0$
6:     **end for**
7:     **for** $\forall v \in \mathcal{N}_s$ **do**   ▷ Saturate all outgoing edges from the source
8:         $d(v) \leftarrow 1$
9:         $f_G(s, v) \leftarrow c(edge(s, v))$
10:         $f_{G^*}(v, s) \leftarrow -c(edge(s, v))$
11:         $e_G(s) \leftarrow -c(edge(s, v))$
12:         $e_G(v) \leftarrow c(edge(s, v))$
13:         Append v to $Active\_node$ ▷ Build the active node list
14:     **end for**
15:     **while** $\text{size}(Active\_node) > 0$ **do**   ▷ While there are active nodes, discharge them
16:         $current\_node \leftarrow \text{pop\_front}(Active\_node)$ ▷ Get the first active node
17:         $state \leftarrow \text{discharge}(current\_node)$
18:         **if** $state == ACTIVE$ **then**   ▷ If node is still active then put it at the end of the list
19:             push($Active\_node$,$current\_node$)
20:         **end if**
21:     **end while**
22:     **return** $e(t)$ ▷ Final flow is equal to the flow entering the sink node
23: **end procedure**

Another popular heuristic is *Global relabel*. In this heuristic, all nodes are periodically labelled from the distance of the node to the sink. This is can be done by runnig a BFS from the sink node t in the residual graph G^*. When used in conjuction with the FIFO heuristic, there's a huge performance speedup. The Global relabel heuristic is expensive to perform so it is only run after every $|\mathcal{V}|$ relabel operations.

The final heuristic we discuss is known as the *Gap relabel*. This heuristic is based on an important observation, nodes can only push to other nodes that are one level lower. Hence, if there are no noded of a certain level, d, then it is not possible for higher nodes, at level $d+1$, to send their flow to the nodes at the next lowest level, $d-1$, hence this gap in the levels allows us to relabel all nodes that are higher than level d to $|\mathcal{V}|$. These relabelled nodes will no more be considered in further push or relabel operations. When the max-flow is determined, graph partitioning can be easily obtained. All nodes that are equal to or higher than the source are part of the source set, i.e $\mathcal{V}_S = \{v \in \mathcal{V} | d(v) \geq |\mathcal{V}|\}$ and $\mathcal{V}_T = \mathcal{V} - \mathcal{V}_S$.

3.4.4   Move Making Algorithms

Modern move making algorithms based on combinatorial graph cuts outperform previous move making methods, such as simulated annealing and ICM, as well as message passing algorithms because of their increased accuracy and efficiency [173]. Specifically, the α-expansion and $\alpha\beta$-swap [122] has become very popular and gained a large acceptance in the vision community [174].

In the α-expansion, the algorithm iteratively makes the move to expand the α-label set. The label that provides the largest decrease in energy for all labels is kept. When no further label changes can be made, then the algorithm has reachde convergence and terminates. In the $\alpha\beta$-swap, the algorithm iteratively chooses two pixel sets with labels α and β and swaps the labels of the pixels within these sets. The swap between the pair of labels that results in the largest decrease in energy is chosen. Similarly, when no more swap moves can be made, the algorithm has reached convergence and terminates. For binary segmentation, both of these algorithms require just one iteration to reach convergence and the optimal move is determined by using graph cuts.

Conclude this chapter? Comparison of Running times for these algorithms?

Chapter 4

Pre-Processing and Post-Processing Scheme for Fluorescence Microscopy Images

4.1 Removal of Artifacts using Connected Components

4.2 Anisotropic Diffusion

4.2.1 Coherence Enhancing Diffusion

4.2.2 Coherence Enhancing Diffusion with Optimised Rotational Invariance

4.3 Poisson Denoising

4.3.1 Total-Variation Denoising

4.4 Contrast Enhancement

Chapter 5

Conclusion and Future Work

Appendix A

Introduction to Graph Theory

Graph A graph G is a pair (V, E), where V is the set of nodes/vertices and E is the set of edges consisting of pairs (u, v) where $u, v \in V$. The graph is assumed to be finite i.e. $|V| = n$ and $|E| = m$.

In an **undirected graph**, the edge (u, v) and (v, u) are not distinct. That is, they refer to the same edge. However, in a **directed graph**, the two edge are now distinct. In a directed graph with edge (u, v), u is known as the **tail** and v is know as the **head**. In directed graphs, edges, also known as arcs, are depicted by placing arrowheads at the head of the edge. Given an edge $e = (u, v)$, u and v are said to be **incident** on e. A graph is said to be **simple** if it does not contain any self-loops. A **self-loop** is an edge with of its end points being the same vertex.
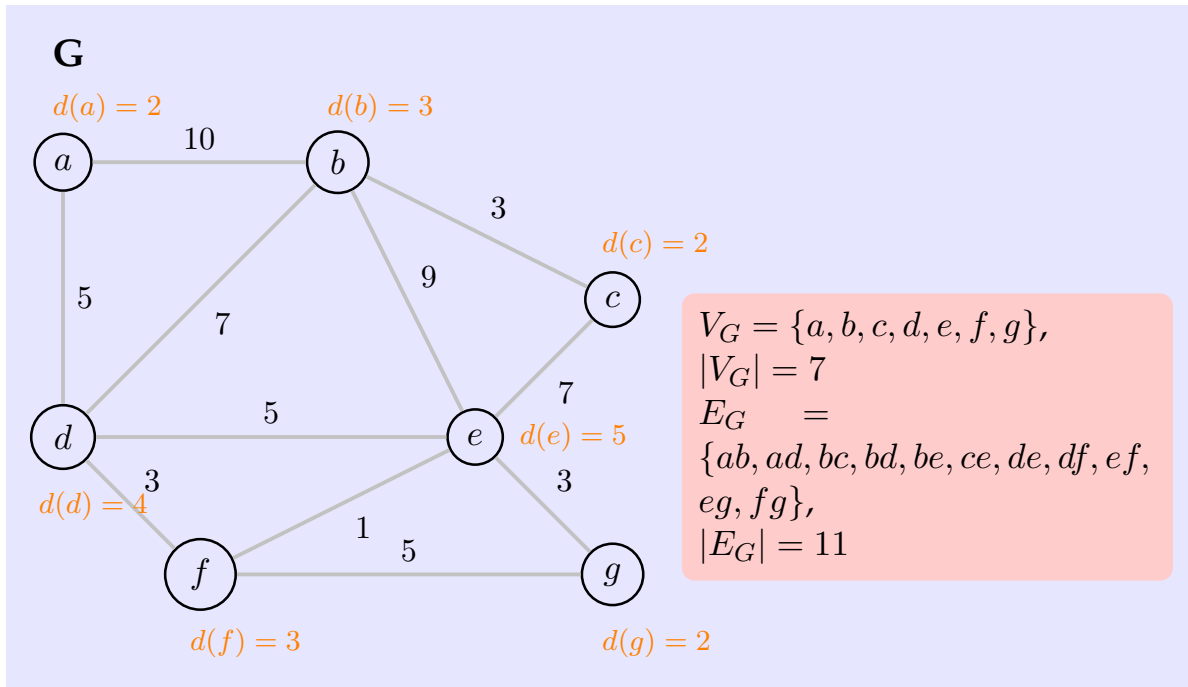

FIGURE A.1: Undirected weighted graph **G**. The degree of each node is shown next to the corresponding node. The graph is simple. The red box shows the vertex set, V_G, and edge set, E_G, and their corresponding norm.

Degree The degree of a vertex v is the number of edges incident on it. $deg(v) = |\{(u, v), (v, u) \in E\}|$. A self-loop counts for 2.

If a graph is directed, also known as a **digraph**, then a node v has an **in-degree** $d_{in}(v)$ and an **out-degree** $d_{out}(v)$. A digraph is said to be **balanced** if $d_{in}(v) = d_{out}(v), \forall v \in V$.
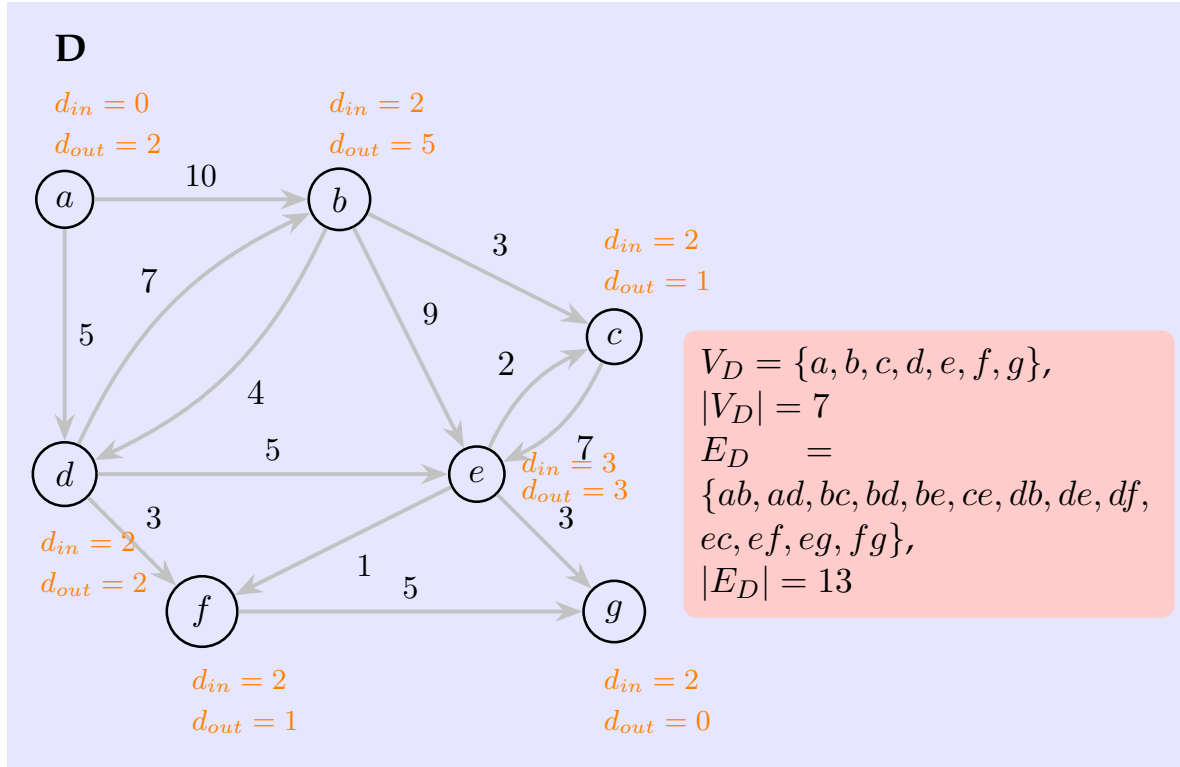
D

FIGURE A.2: Directed weighted graph (Digraph) **D**. The in-degree and out-degree is shown next to each node. The graph is simple and not balanced. The red box shows the vertex set, V_D, and edge set, E_D, and their corresponding norm.

Subgraph A graph $G' = (V', E')$ is said to be a sub-graph of $G = (V, E)$, denoted as $G' \subseteq G$, if $V' \subseteq V$ and $E' \subseteq E$.
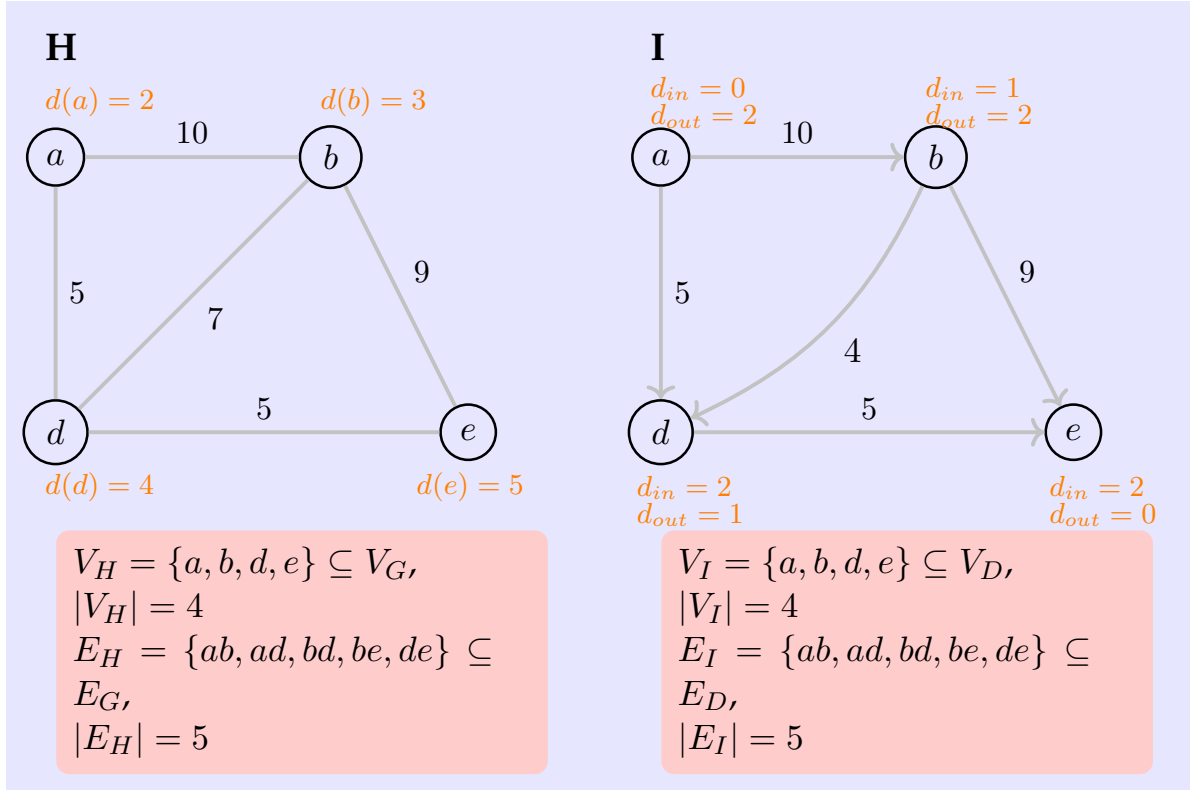
Clique A clique is a maximal subgraph.

$$V_H = \{a, b, d, e\} \subseteq V_G,$$
$$|V_H| = 4$$
$$E_H = \{ab, ad, bd, be, de\} \subseteq E_G,$$
$$|E_H| = 5$$

$$V_I = \{a, b, d, e\} \subseteq V_D,$$
$$|V_I| = 4$$
$$E_I = \{ab, ad, bd, be, de\} \subseteq E_D,$$
$$|E_I| = 5$$

FIGURE A.3: Undirected weighted graph **H** is a subgraph of **G** in Figure XX, **H** $\subseteq$ **G**. Directed weighted graph **I** is a subgraph of **D** in Figure XX, **I** $\subseteq$ **D**. The degree of each node is shown next to the corresponding node. The red box shows the vertex set, the edge set and their corresponding norms.

$$V_G = \{a, b, c, d, e, f, g\},$$
$$E_G = \{ab, ad, bc, bd, be, ce, de, df, ef,$$
$$eg, fg\},$$
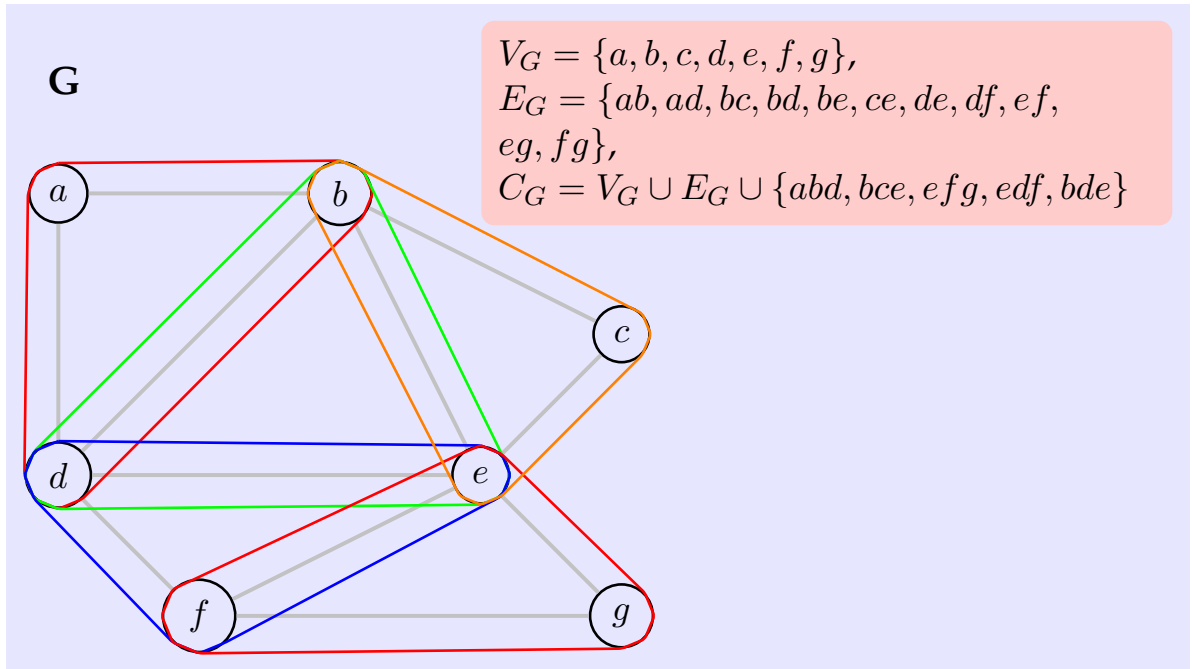$$C_G = V_G \cup E_G \cup \{abd, bce, efg, edf, bde\}$$

FIGURE A.4: Cliques of the undirected weighted graph **G**. The maximal cliques are shown by the hyperedges that encompass the nodes of that clique.

Bibliography

[1] Kenneth R. Spring. *Encyclopedia of Optical Engineering - Fluorescence Microscopy*. 270 Madison Avenue, New York, New York 10016: Marcel Dekker, Inc., 2003, pp. 548–555. DOI: 10.1081/E-EOE.

[2] Ondřej Daněk. "Graph Cut Based Image Segmentation in Fluorescence Microscopy [online]". Doctoral theses, Dissertations. Masaryk University, Faculty of Informatics, Brno, 2012 [cit. 2016-09-08]. URL: http://is.muni.cz/th/60931/fi_d/thesis-final.pdf.

[3] Jan Hubený. "Applications of PDE - Based Image Processing in Fluorescence Microscopy [online]". Doctoral theses, Dissertations. Masaryk University, Faculty of Informatics, Brno, 2008 [cit. 2016-09-07]. URL: http://is.muni.cz/th/4012/fi_d/.

[4] Fatima A. Merchant and Ammasi Periasamy. "Fluorescence Imaging". In: *Microscope Image Processing*. USA: Elsevier Inc, 2008, pp. 247–271. ISBN: 978-0-12-372578-3.

[5] Pavel Matula. "Image Processing in Fluorescence Microscopy and its Utilization in Cell Biology Experiments [online]". Doctoral theses, Dissertations. Masaryk University, Faculty of Informatics, Brno, 2012 [cit. 2016-09-09].

[6] Karl-Friedrich Koch. *Fluorescence Microscopy - Instruments, Methods, Applications*. Lietz Wetzlar, 1972.

[7] Andrew Vaughan. *Principles of Fluorescence Microscopy*. Document. (accessed September 6, 2016).

[8] Pinaki Sarder and Arye Nehorai. "Deconvolution Methods for 3-D Fluorescence Microscopy Images". In: *IEEE Signal Processing Magazine* 23.3 (2006), 32—45. DOI: 10.1046/j.1365-2818.2000.00754.x.

[9] Mortimer Abramowitz and Michael W. Davidson. *Introduction to Fluorescence*. Website. (accessed September 6, 2016). URL: http://www.olympusmicro.com/primer/lightandcolor/fluorointroduction.html.

[10] Kenneth R. Spring and Michael W. Davidson. *Introduction to Fluorescence Microscopy*. Website. (accessed September 6, 2016). URL: http://www.microscopyu.com/techniques/fluorescence/introduction-to-fluorescence-microscopy.

[11] Jurek W. Dobrucki. "Fluorescence Microscopy". In: *Fluorescence Microscopy: From Principles to Biological Applications*. 1st Edition. Wiley-VCH Verlag GmbH & Co., 2013, pp. 97–142.

[12] Nobel Media AB. *The Fluorescence Microscopy*. Website. (accessed September 6, 2016). URL: http://www.nobelprize.org/educational/physics/microscopes/fluorescence/.

[13] *Fluorescence SpectraViewer*. Website. (accessed September 18, 2016). URL: https://www.thermofisher.com/us/en/home/life-science/cell-analysis/labeling-chemistry/fluorescence-spectraviewer.html.

[14] Roger Y. Tsien. "The Green Fluorescent Protein". In: *Annual Review of Biochemistry* 67 (1998), pp. 509–544.

[15] Michal Kozubek. "FISH imaging". In: *Confocal and Two-Photon Microscopy: Foundations, Applications and Advances* (2001), 389—429.

[16] Z. Theodosiou et al. "Automated Analysis of FISH and immunohistochemistry images: A Review". In: *Cytometry Part A* 71.7 (2007), pp. 439–450.

[17] Rudolf Amann and Bernhard M. Fuchs. "Single-cell identification in microbial communities by improved fluorescence in situ hybridization techniques". In: *Nature Reviews Microbiology* 6.5 (2008), 339—348. DOI: 10.1038/nrmicro1888.

[18] Kelly Cude and Kelly Burke. "Introduction to Fluorescence Microscopy". In: (14 July 2012).

[19] Kishore Reddy Katikireddy and Finbarr O'Sullivan. "Immunohistochemical and Immunofluorescence Procedures for Protein Analysis". In: *Gene Expression Profiling: Methods and Protocols*. Ed. by Lorraine O'Driscoll. Totowa, NJ: Humana Press, 2011, pp. 155–167. ISBN: 978-1-61779-289-2. DOI: 10.1007/978-1-61779-289-2_11. URL: http://dx.doi.org/10.1007/978-1-61779-289-2_11.

[20] Jeff W. Lichtman and José-Angel Conchello. *Nature Methods - Fluorescence microscopy*. Vol. 2. 12. Nature Publishing Group, Decmeber 2005, pp. 910–919. DOI: 10.1038/NMETH817. URL: http://www.nature.com/naturemethods.

[21] Paul D. Andrews, Ian S. Harper, and Jason R. Swedlow. "To 5D and Beyond: Quantitative Fluorescence Microscopy in the Postgenomic Era". In: *Traffic*. Vol. 3. Munksgaard International Publishers, 2002, pp. 29–36.

[22] George Rice. *Fluorescent Microscopy*. Website. (accessed September 6, 2016). URL: http://serc.carleton.edu/microbelife/research_methods/microscopy/fluromic.html.

[23] Kavita Aswani, Tushare Jinadasa, and Claire M. Brown. "Fluorescence Microscopy Light Sources". In: *Microscopy Today*. 2012, pp. 22–28. DOI: 10.1017/S1551929512000399. URL: www.microscopy-today.com.

[24] Thermo Fisher Scientific. *Fundamentals of Fluorescence Microscopy*. Website. (accessed September 6, 2016). URL: https://www.thermofisher.com/us/en/home/life-science/cell-analysis/cell-analysis-learning-center/molecular-probes-school-of-fluorescence/fundamentals-of-fluorescence-microscopy.html.

[25] Douglas B. Murphy. *Fundamentals of Light Microscopy and Electronic Imaging*. 2nd Edition. USA: John Wiley & Sons, Inc., 2001. ISBN: 0-471-25391-X.

[26] Ian T. Young. "Shading Correction: Compensation for Illumination and Sensor Inhomogeneities". In: *Current Protocols in Cytometry*. John Wiley & Sons, Inc., 2001. ISBN: 9780471142959. DOI: 10.1002/0471142956.cy0211s14. URL: http://dx.doi.org/10.1002/0471142956.cy0211s14.

[27] Ghauharali, Hofstraat, and Brakenhoff. "Fluorescence photobleaching-based shading correction for fluorescence microscopy". In: *Journal of Microscopy* 192.2 (1998), pp. 99–113. ISSN: 1365-2818. DOI: 10.1046/j.1365-2818.1998.00412.x. URL: http://dx.doi.org/10.1046/j.1365-2818.1998.00412.x.

[28] Michael Model. "Intensity Calibration and Flat-Field Correction for Fluorescence Microscopes". In: *Current Protocols in Cytometry*. John Wiley & Sons, Inc., 2001. ISBN: 9780471142959. DOI: `10.1002/0471142956.cy1014s68`. URL: `http://dx.doi.org/10.1002/0471142956.cy1014s68`.

[29] Michael A. Model and Janis K. Burkhardt. "A standard for calibration and shading correction of a fluorescence microscope". In: *Cytometry* 44.4 (2001), pp. 309–316. ISSN: 1097-0320. DOI: `10.1002/1097-0320(20010801)44:4<309::AID-CYTO1122>3.0.CO;2-3`. URL: `http://dx.doi.org/10.1002/1097-0320(20010801)44:4<309::AID-CYTO1122>3.0.CO;2-3`.

[30] Anne Carpenter. *CIL 21739*. Picture. (accessed September 9, 2016). URL: `http://www.cellimagelibrary.org/images/21739`.

[31] Stephen A. Boppart et al. "Optical probes and techniques for molecular contrast enhancement in coherence imaging". In: *Journal of Biomedical Optics* 10.4 (2005), pp. 041208–041208–14. DOI: `10.1117/1.2008974`. URL: `http://dx.doi.org/10.1117/1.2008974`.

[32] Molecular Expressions. *Photobleaching*. Picture. (accessed September 9, 2016). URL: `http://micro.magnet.fsu.edu/primer/java/fluorescence/photobleaching/`.

[33] Margret Keuper. "Segmentation of Cells and Sub-cellular Structures from Microscopic Recordings [online]". Doctoral theses, Dissertations. Albert-Ludwigs-Universität, 2012 [cit. 2016-09-12]. URL: `http://lmb.informatik.uni-freiburg.de/Publications/2012/Keu12/Dissertation_Keuper.pdf`.

[34] Arjan Tibbe. *CIL 40968*. Picture. (accessed September 9, 2016). URL: `http://www.cellimagelibrary.org/images/40968`.

[35] Eran A. Mukamel, Hazen Babcock, and Xiaowei Zhuang. "Statistical Deconvolution for Superresolution Fluorescence Microscopy". In: *Biophysical Journal* 102.10 (2012), pp. 2391–2400. DOI: `10.1038/srep09894`. URL: `http://dx.doi.org/10.1016/j.bpj.2012.03.070`.

[36] Peter J Verveer et al. "High-resolution three-dimensional imaging of large specimens with light sheet–based microscopy". In: *Nature Methods* 4 (2007), pp. 311–313. DOI: `10.1038/nmeth1017`. URL: `http://www.nature.com/nmeth/journal/v4/n4/abs/nmeth1017.html`.

[37] Ammassi Periasamy, Paul Skoglundand Colten Noakes, and Raymond Keller. "An Evaluation of Two-Photon Excitation Versus Confocal and Digital Deconvolution Fluorescence Microscopy Imaging in Xenopus Morphogenesis". In: *Microscopy Research and Technique* 4 (2007), pp. 311–313. DOI: `10.1038/nmeth1017`. URL: `http://www.nature.com/nmeth/journal/v4/n4/abs/nmeth1017.html`.

[38] Jason R. Swedlow. "Quantitative Fluorescence Microscopy and Image Deconvolution". In: *Digital Microscopy, 3rd Edition*. Vol. 81. Methods in Cell Biology. Academic Press, 2007, pp. 447–465. DOI: `http://dx.doi.org/10.1016/S0091-679X(06)81021-6`. URL: `http://www.sciencedirect.com/science/article/pii/S0091679X06810216`.

[39]   Johan J. de Rooi, Cyril Ruckebusch, and Paul H. C. Eilers. "Sparse Deconvolution in One and Two Dimensions: Applications in Endocrinology and Single-Molecule Fluorescence Imaging". In: *Analytical Chemistry* 86.13 (2014). PMID: 24893114, pp. 6291–6298. DOI: 10.1021/ac500260h. eprint: http://dx.doi.org/10.1021/ac500260h. URL: http://dx.doi.org/10.1021/ac500260h.

[40]   Alexander Wong, Xiao Yu Wang, and Maud Gorbet. "Bayesian-based deconvolution fluorescence microscopy using dynamically updated nonstationary expectation estimates". In: *Scientific Reports* 5.10849 (2015), pp. 1–9. DOI: 10.1038/srep10849. URL: http://dx.doi.org/10.1038/srep10849.

[41]   Boyoung Kim and Takeshi Naemura. "Blind Depth-variant Deconvolution of 3D Data in Wide-field Fluorescence Microscopy". In: *Scientific Reports* 5.9894 (2015), pp. 1–9. DOI: 10.1038/srep09894. URL: http://dx.doi.org/10.1038/srep09894.

[42]   Jing Qin et al. "Detail-preserving Fluorescence Microscopy Image Deconvolution". In: *Conference on Lasers and Electro-Optics*. Optical Society of America, 2016, STh4G.7. DOI: 10.1364/CLEO_SI.2016.STh4G.7. URL: http://www.osapublishing.org/abstract.cfm?URI=CLEO_SI-2016-STh4G.7.

[43]   Ryan Naidoo anad Jules-Raymond Tapamo. "A Preprocessing Scheme for Fluorescence Microscopy Image Segmentation". In: *International Journal of Imaging and Robotics* 16.4 (2016), pp. 1–23. ISSN: ISSN 2231–525X.

[44]   Gijsbert Michiel Peter Van Kempen. "Image Restoration in Fluorescence Microscopy [online]". Doctoral theses, Dissertations. Technische Universiteit Delft, 1999 [cit. 2016-09-08]. URL: http://www.tnw.tudelft.nl/fileadmin/Faculteit/TNW/Over_de_faculteit/Afdelingen/Imaging_Science_and_Technology/Research/Research_Groups/Quantitative_Imaging/Publications/List_Publications/doc/thesis_kempen.pdf.

[45]   Erik Meijering. "Cell Segmentation: 50 Years Down the Road [Life Sciences]". In: *IEEE Signal Processing Magazine* 29.5 (2012), pp. 140–145. ISSN: 1053-5888. DOI: 10.1109/MSP.2012.2204190.

[46]   Bruce Alberts et al. *Molecular Biology of the Cell*. 5th Edition. New York, NY, USA: Garland Science, 2007. ISBN: 9780815341055.

[47]   Cédrik Vonesch et al. "The Colored Revolution of Bioimaging [An introduction to fluorescence microscopy]". In: *IEEE Signal Processing Magazine* 29.5 (2006), pp. 20–31.

[48]   Ewert Bengtsson, Carolina Wählby, and Joakim Lindblad. "Robust cell image segmentation methods". In: *Pattern Recognition and Image Analysis: Advances in Mathematical Theory and Applications* 14.52 (2004), pp. 157–167. ISSN: 1054-6618.

[49]   W.E. Tolles. "Section of Biology: The Cytoanalyzer—An Example of Physics in Medical Research*". In: *Transactions of the New York Academy of Sciences* 17.3 Series II (1955), pp. 250–256. ISSN: 2164-0947. DOI: 10.1111/j.2164-0947.1955.tb01204.x. URL: http://dx.doi.org/10.1111/j.2164-0947.1955.tb01204.x.

[50]   Judith M. S. Prewitt and Mortimer L. Mendelsohn. "The Analysis of Cell Images*". In: *Annals of the New York Academy of Sciences* 128.3 (1966), pp. 1035–1053. ISSN: 1749-6632. DOI: 10.1111/j.1749-6632.1965.tb11715.x. URL: http://dx.doi.org/10.1111/j.1749-6632.1965.tb11715.x.

[51]   Metin N. Gurcan et al. "Histopathological image analysis: A review". In: *IEEE Reviews in Biomedical Engineering* (2009), pp. 147–171.

[52] Alden A. Dima et al. "Comparison of segmentation algorithms for fluorescence microscopy images of cells". In: *Cytometry Part A* 79A.7 (2011), pp. 545–559. ISSN: 1552-4930. DOI: 10.1002/cyto.a.21079. URL: http://dx.doi.org/10.1002/cyto.a.21079.

[53] Z. Pincus and J.A. Theriot. "Comparison of quantitative methods for cell-shape analysis". In: *Journal of Microscopy* 227.2 (2007), pp. 140–156. ISSN: 1365-2818. DOI: 10.1111/j.1365-2818.2007.01799.x. URL: http://dx.doi.org/10.1111/j.1365-2818.2007.01799.x.

[54] Luís Pedro Coelho, Aabid Shariff, and Robert F. Murphy. "Nuclear Segmentation in Microscope Cell Images: A Hand-Segmented Dataset and Comparison of Algorithms". In: *Proc IEEE Int Symp Biomed Imaging* 5.193098E6.2 (2009), pp. 518–521. ISSN: 1365-2818. DOI: 10.1111/j.1365-2818.2007.01799.x. URL: http://www.ncbi.nlm.nih.gov/pmc/articles/PMC2901896/.

[55] Qiang Wu, Fatima A. Merchant, and Kenneth R. Castleman. *Encyclopedia of Optical Engineering - Fluorescence Microscopy*. 1st Edition. Elsevier Inc., 2008. ISBN: 978-0-12-372578-3.

[56] E. Meijering et al. "Design and validation of a tool for neurite tracing and analysis in fluorescence microscopy images". In: *Cytometry Part A* 58A.2 (2004), pp. 167–176. ISSN: 1552-4930. DOI: 10.1002/cyto.a.20022. URL: http://dx.doi.org/10.1002/cyto.a.20022.

[57] Quanli Wang et al. "Image segmentation and dynamic lineage analysis in single-cell fluorescence microscopy". In: *Cytometry Part A* 77A.1 (2010), pp. 101–110. ISSN: 1552-4930. DOI: 10.1002/cyto.a.20812. URL: http://dx.doi.org/10.1002/cyto.a.20812.

[58] Rafael C. Gonzalez and Richard E. Woods. *Digital Image Processing*. 3rd Edition. New Jersey, USA: Prentice Hall, Inc., 2002.

[59] L.B. Dorini, R. Minetto, and N. J. Leite. "White blood cell segmentation using morphological operators and scale-space analysis". In: *Computer Graphics and Image Processing, 2007. SIBGRAPI 2007. XX Brazilian Symposium on*. 2007, pp. 294–304. DOI: 10.1109/SIBGRAPI.2007.33.

[60] D. Anoraganingrum. "Cell segmentation with median filter and mathematical morphology operation". In: *Image Analysis and Processing, 1999. Proceedings. International Conference on*. 1999, pp. 1043–1046. DOI: 10.1109/ICIAP.1999.797734.

[61] B.R. Kumar, D.K. Joseph, and T.V. Sreenivas. "Teager energy based blood cell segmentation". In: *Digital Signal Processing, 2002. DSP 2002. 2002 14th International Conference on*. Vol. 2. 2002, pp. 619–622. DOI: 10.1109/ICDSP.2002.1028167.

[62] Kan Jiang, Qing-Min Liao, and Sheng-Yang Dai. "A novel white blood cell segmentation scheme using scale-space filtering and watershed clustering". In: *Machine Learning and Cybernetics, 2003 International Conference on*. Vol. 5. 2003, pp. 2820–2825. DOI: 10.1109/ICMLC.2003.1260033.

[63] Gang Lin et al. "A hybrid 3D watershed algorithm incorporating gradient cues and object models for automatic segmentation of nuclei in confocal image stacks". In: *Cytometry Part A* 56A.1 (2003), pp. 23–36. ISSN: 1552-4930. DOI: 10.1002/cyto.a.10079. URL: http://dx.doi.org/10.1002/cyto.a.10079.

[64]   Michael Kass, Andrew Witkin, and Demetri Terzopoulos. "Snakes: Active contour models". In: *International Journal of Computer Vision* 1.4 (1988), pp. 321–331.

[65]   Vicent Caselles, Ron Kimmel, and Guillermo Sapiro. "Geodesic Active Contours". In: *International Journal of Computer Vision* 22.1 (1997), pp. 61–79. ISSN: 0920-5691. DOI: 10.1023/A:1007979827043. URL: http://dx.doi.org/10.1023/A:1007979827043.

[66]   Hongsheng Li et al. "Automated actin filament segmentation, tracking and tip elongation measurements based on open active contour models". In: *2009 IEEE International Symposium on Biomedical Imaging: From Nano to Macro*. 2009, pp. 1302–1305. DOI: 10.1109/ISBI.2009.5193303.

[67]   J. Cheng and J. C. Rajapakse [ast]. "Segmentation of Clustered Nuclei With Shape Markers and Marking Function". In: *IEEE Transactions on Biomedical Engineering* 56.3 (2009), pp. 741–748. ISSN: 0018-9294. DOI: 10.1109/TBME.2008.2008635.

[68]   Stanley Osher and Ronald P. Fedkiw. *Level set methods and dynamic implicit surfaces*. Applied mathematical science. New York, N.Y.: Springer, 2003. ISBN: 0-387-95482-1. URL: http://opac.inria.fr/record=b1099358.

[69]   O. Dzyubachyk, W. Niessen, and E. Meijering. "Advanced level-set based multiple-cell segmentation and tracking in time-lapse fluorescence microscopy images". In: *2008 5th IEEE International Symposium on Biomedical Imaging: From Nano to Macro*. 2008, pp. 185–188. DOI: 10.1109/ISBI.2008.4540963.

[70]   C. Ortiz de Solórzano et al. "Segmentation of nuclei and cells using membrane related protein markers". In: *Journal of Microscopy* 201 (2001), pp. 404–415.

[71]   Alexandre Dufour et al. "Segmenting and tracking fluorescent cells in dynamic 3-D microscopy with coupled active surfaces." In: *IEEE Transactions on Image Processing* 14.9 (2005), pp. 1396–410. URL: https://hal.archives-ouvertes.fr/hal-00014483.

[72]   Oleh Dzyubachyk et al. "Advanced Level-Set-Based Cell Tracking in Time-Lapse Fluorescence Microscopy." In: *IEEE Trans. Med. Imaging* 29.3 (2010), pp. 852–867. URL: http://dblp.uni-trier.de/db/journals/tmi/tmi29.html#DzyubachykCENM10.

[73]   Fatima Boukari and Sokratis Makrogiannis. "Spatio-temporal Level-Set Based Cell Segmentation in Time-Lapse Image Sequences". In: *Advances in Visual Computing: 10th International Symposium, ISVC 2014, Las Vegas, NV, USA, December 8-10, 2014, Proceedings, Part II*. Ed. by George Bebis et al. Cham: Springer International Publishing, 2014, pp. 41–50. ISBN: 978-3-319-14364-4. DOI: 10.1007/978-3-319-14364-4_5. URL: http://dx.doi.org/10.1007/978-3-319-14364-4_5.

[74]   Martin Maška et al. "A Comparison of Fast Level Set-Like Algorithms for Image Segmentation in Fluorescence Microscopy". In: *Advances in Visual Computing: Third International Symposium, ISVC 2007, Lake Tahoe, NV, USA, November 26-28, 2007, Proceedings, Part II*. Ed. by George Bebis et al. Berlin, Heidelberg: Springer Berlin Heidelberg, 2007, pp. 571–581. ISBN: 978-3-540-76856-2. DOI: 10.1007/978-3-540-76856-2_56. URL: http://dx.doi.org/10.1007/978-3-540-76856-2_56.

[75] Ondřej Daněk et al. "Segmentation of Touching Cell Nuclei Using a Two-Stage Graph Cut Model". In: *Image Analysis: 16th Scandinavian Conference, SCIA 2009, Oslo, Norway, June 15-18, 2009. Proceedings*. Ed. by Arnt-Børre Salberg, Jon Yngve Hardeberg, and Robert Jenssen. Berlin, Heidelberg: Springer Berlin Heidelberg, 2009, pp. 410–419. ISBN: 978-3-642-02230-2. DOI: 10.1007/978-3-642-02230-2_42. URL: http://dx.doi.org/10.1007/978-3-642-02230-2_42.

[76] C. Chen et al. "Constraint factor graph cut–based active contour method for automated cellular image segmentation in RNAi screening". In: *Journal of Microscopy* 230.2 (2008), pp. 177–191. ISSN: 1365-2818. DOI: 10.1111/j.1365-2818.2008.01974.x. URL: http://dx.doi.org/10.1111/j.1365-2818.2008.01974.x.

[77] Y. Al-Kofahi et al. "Improved Automatic Detection and Segmentation of Cell Nuclei in Histopathology Images". In: *IEEE Transactions on Biomedical Engineering* 57.4 (2010), pp. 841–852. ISSN: 0018-9294. DOI: 10.1109/TBME.2009.2035102.

[78] H. Kong, M. Gurcan, and K. Belkacem-Boussaid. "Partitioning Histopathological Images: An Integrated Framework for Supervised Color-Texture Segmentation and Cell Splitting". In: *IEEE Transactions on Medical Imaging* 30.9 (2011), pp. 1661–1677. ISSN: 0278-0062. DOI: 10.1109/TMI.2011.2141674.

[79] Huei-Fang Yang and Yoonsuck Choe. "Cell tracking and segmentation in electron microscopy images using graph cuts". In: *2009 IEEE International Symposium on Biomedical Imaging: From Nano to Macro*. 2009, pp. 306–309. DOI: 10.1109/ISBI.2009.5193045.

[80] L. Zhang et al. "Automated segmentation of abnormal cervical cells using global and local graph cuts". In: *2014 IEEE 11th International Symposium on Biomedical Imaging (ISBI)*. 2014, pp. 485–488. DOI: 10.1109/ISBI.2014.6867914.

[81] Lu Liu et al. "Interactive Separation of Segmented Bones in CT Volumes Using Graph Cut". In: *Medical Image Computing and Computer-Assisted Intervention – MICCAI 2008: 11th International Conference, New York, NY, USA, September 6-10, 2008, Proceedings, Part I*. Ed. by Dimitris Metaxas et al. Berlin, Heidelberg: Springer Berlin Heidelberg, 2008, pp. 296–304. ISBN: 978-3-540-85988-8. DOI: 10.1007/978-3-540-85988-8_36. URL: http://dx.doi.org/10.1007/978-3-540-85988-8_36.

[82] Nhat Vu and B.S. Manjunath. "Graph cut segmentation of neuronal structures from transmission electron micrographs". In: *IEEE International Conference on Image Processing* (2008).

[83] H. P. Ng et al. "Medical Image Segmentation Using K-Means Clustering and Improved Watershed Algorithm". In: *2006 IEEE Southwest Symposium on Image Analysis and Interpretation*. 2006, pp. 61–65. DOI: 10.1109/SSIAI.2006.1633722.

[84] Kalpana Shrivastava, Neelesh Gupta, and Neetu Sharma. "Medical Image Segmentation using Modified K Means Clustering". In: *International Journal of Computer Applications* 103.16 (2014), pp. 12–16. ISSN: 0975-8887. DOI: 10.1109/TMI.2011.2141674.

[85] Nameirakpam Dhanachandra, Khumanthem Manglem, and Yambem Jina Chanu. "Image Segmentation Using K -means Clustering Algorithm and Subtractive Clustering Algorithm". In: *Procedia Computer Science* 54 (2015), pp. 764–771. ISSN: 1877-0509. DOI: http://dx.doi.org/10.1016/j.procs.2015.06.090. URL: http://www.sciencedirect.com/science/article/pii/S1877050915014143.

[86] Xiaowei Chen, Xiaobo Zhou, and S.T.C. Wong. "Automated segmentation, classification, and tracking of cancer cell nuclei in time-lapse microscopy". In: *IEEE Transactions on Biomedical Engineering* 53.4 (2006), pp. 762–766. ISSN: 0018-9294. DOI: 10.1109/TBME.2006.870201.

[87] Jihong Liu, Weina Ma, and Soo-Young Lee. "A Segmentation Method Based on Dynamic Programming for Breast Mass in MRI Images". In: *Medical Biometrics: First International Conference, ICMB 2008, Hong Kong, China, January 4-5, 2008. Proceedings*. Ed. by David Zhang. Berlin, Heidelberg: Springer Berlin Heidelberg, 2007, pp. 307–313. ISBN: 978-3-540-77413-6. DOI: 10.1007/978-3-540-77413-6_39. URL: http://dx.doi.org/10.1007/978-3-540-77413-6_39.

[88] Y. Zhang, B. J. Matuszewski, and L. K. Shark. "A Novel Medical Image Segmentation Method using Dynamic Programming". In: *Medical Information Visualisation - BioMedical Visualisation, 2007. MediVis 2007. International Conference on*. 2007, pp. 69–74.

[89] R. Cardenes et al. "K-Voronoi diagrams computing in arbitrary domains". In: *Image Processing, 2003. ICIP 2003. Proceedings. 2003 International Conference on*. Vol. 2. 2003, pp. 941–944. DOI: 10.1109/ICIP.2003.1246838.

[90] Chunyan Jiang, Xinhua Zhang, and Christoph Meinel. "Hybrid Framework for Medical Image Segmentation". In: *Computer Analysis of Images and Patterns: 11th International Conference, CAIP 2005, Versailles, France, September 5-8, 2005. Proceedings*. Ed. by André Gagalowicz and Wilfried Philips. Berlin, Heidelberg: "Springer Berlin Heidelberg, 2005, pp. 264–271. ISBN: 978-3-540-32011-1. DOI: 10.1007/11556121_33. URL: http://dx.doi.org/10.1007/11556121_33.

[91] G. Li et al. "Segmentation of Touching Cells Using Gradient Flow Tracking". In: *2007 4th IEEE International Symposium on Biomedical Imaging: From Nano to Macro*. 2007, pp. 77–80. DOI: 10.1109/ISBI.2007.356792.

[92] Fatima A. Merchant, Shishir K. Shah, and Kenneth R. Castleman. "Object Measurement". In: *Microscope Image Processing*. USA: Elsevier Inc, 2008, pp. 195–219. ISBN: 978-0-12-372578-3.

[93] Charlotte Giesen et al. "Highly multiplexed imaging of tumor tissues with subcellular resolution by mass cytometry". In: *Nature Methods* 11.4 (2014), pp. 417–422. DOI: 10.1038/nmeth.2869. URL: http://dx.doi.org/10.1038/nmeth.2869.

[94] Xiaosong Yuan et al. "MDL Constrained 3-D Grayscale Skeletonization Algorithm for Automated Extraction of Dendrites and Spines from Fluorescence Confocal Images". In: *Neuroinformatics* 7.4 (2009), pp. 213–232. ISSN: 1559-0089. DOI: 10.1007/s12021-009-9057-y. URL: http://dx.doi.org/10.1007/s12021-009-9057-y.

[95] Michal Kozubek and Pavel Matula. "An efficient algorithm for measurement and correction of chromatic aberrations in fluorescence microscopy". In: *Journal of Microscopy* 200.3 (2000), pp. 206–217. ISSN: 1365-2818. DOI: 10.1046/j.1365-2818.2000.00754.x. URL: http://dx.doi.org/10.1046/j.1365-2818.2000.00754.x.

[96] Dominique Attali and Annick Montanvert. "Computing and Simplifying 2D and 3D Continuous Skeletons". In: *Elsevier Computer Vision and Image Understanding* 67.3 (1997), pp. 261–273. ISSN: 1365-2818. DOI: 10.1006/cviu.1997.0536. URL: http://dx.doi.org/10.1046/j.1365-2818.2000.00754.x.

[97] Andrew P. French et al. "Colocalization of fluorescent markers in confocal microscope images of plant cells". In: *Nat. Protocols* 3 (4 2008), pp. 619–628. ISSN: 1754-2189. DOI: 10.1038/nprot.2008.31. URL: http://dx.doi.org/10.1038/nprot.2008.31.

[98] Vadim Zinchuk, Olga Zinchuk, and Teruhiko Okada. "Quantitative Colocalization Analysis of Multicolor Confocal Immunofluorescence Microscopy Images: Pushing Pixels to Explore Biological Phenomena". In: *ACTA HISTOCHEMICA ET CYTOCHEMICA* 40.4 (2007), pp. 101–111. DOI: 10.1267/ahc.07002.

[99] D. Pinkel, T. Straume, and J.W. Gray. "Cytogenetic analysis using quantitative, high-sensitivity, fluorescence hybridization". In: *Proceedings of the National Academy of Sciences* 83.9 (1986), pp. 2934–2938. eprint: http://www.pnas.org/content/83/9/2934.full.pdf. URL: http://www.pnas.org/content/83/9/2934.abstract.

[100] M. Loferer-Krößbacher, J. Klima, and R. Psenner. "Determination of Bacterial Cell Dry Mass by Transmission Electron Microscopy and Densitometric Image Analysis". In: *Appl. Environ. Microbiol.* 64 (2 1998), pp. 688–694. DOI: 10.1038/nmeth929. URL: http://dx.doi.org/10.1038/nmeth929.

[101] N. Watanabe et al. "Motility of bile canaliculi in the living animal: implications for bile flow." In: *The Journal of Cell Biology* 113.5 (1991), pp. 1069–1080. DOI: 10.1083/jcb.113.5.1069. eprint: http://jcb.rupress.org/content/113/5/1069.full.pdf+html. URL: http://jcb.rupress.org/content/113/5/1069.abstract.

[102] Michael J. Rust, Mark Bates, and Xiaowei Zhuang. "Sub-diffraction-limit imaging by stochastic optical reconstruction microscopy (STORM)". In: *Nat Meth* 3 (10 2006), pp. 793–796. DOI: 10.1038/nmeth929. URL: http://dx.doi.org/10.1038/nmeth929.

[103] Michael V. Boland and Robert F. Murphy. "A neural network classifier capable of recognizing the patterns of all major subcellular structures in fluorescence microscope images of HeLa cells". In: *Bioinformatics* 17.12 (2001), pp. 1213–1223. DOI: 10.1093/bioinformatics/17.12.1213. eprint: http://bioinformatics.oxfordjournals.org/content/17/12/1213.full.pdf+html. URL: http://bioinformatics.oxfordjournals.org/content/17/12/1213.abstract.

[104] R.O. Duda, P.E. Hart, and D.G. Stork. *Pattern Classification*. John Wiley & Sons, 2001.

[105] V. Atlamazoglou et al. "Texture analysis of fluorescence microscopic images of colonic tissue sections". In: *Medical and Biological Engineering and Computing* 39.2 (2001), pp. 145–151. ISSN: 1741-0444. DOI: 10.1007/BF02344796. URL: http://dx.doi.org/10.1007/BF02344796.

[106] Riccardo Cicchi et al. "Scoring of collagen organization in healthy and diseased human dermis by multiphoton microscopy". In: *Journal of Biophotonics* 3.1-2 (2010), pp. 34–43. ISSN: 1864-0648. DOI: 10.1002/jbio.200910062. URL: http://dx.doi.org/10.1002/jbio.200910062.

[107] Erik J. Sánchez, Lukas Novotny, and Xie Sunney. "Near-Field Fluorescence Microscopy Based on Two-Photon Excitation with Metal Tips". In: *Phys. Rev. Lett.* 82 (20 1999), pp. 4014–4017. DOI: 10.1103/PhysRevLett.82.4014. URL: http://link.aps.org/doi/10.1103/PhysRevLett.82.4014.

[108] C. Xu et al. "Multiphoton fluorescence excitation: new spectral windows for biological nonlinear microscopy". In: *Proceedings of the National Academy of Sciences* 93.20 (1996), pp. 10763–10768. eprint: http://www.pnas.org/content/93/20/10763.full.pdf. URL: http://www.pnas.org/content/93/20/10763.abstract.

[109] Rajesh Babu Sekar and Ammasi Periasamy. "Fluorescence resonance energy transfer (FRET) microscopy imaging of live cell protein localizations". In: *Journal of Cellular Biology* 160 (5 2004), pp. 629–633. DOI: 10.1083/jcb.200210140.

[110] Mark J. Miller et al. "Two-Photon Imaging of Lymphocyte Motility and Antigen Response in Intact Lymph Node". In: *Science* 296.5574 (2002), pp. 1869–1873. ISSN: 0036-8075. DOI: 10.1126/science.1070051. eprint: http://science.sciencemag.org/content/296/5574/1869.full.pdf. URL: http://science.sciencemag.org/content/296/5574/1869.

[111] Anshu Bagga Mathur, George A. Truskey, and W. Monty Reichert. "Atomic Force and Total Internal Reflection Fluorescence Microscopy for the Study of Force Transmission in Endothelial Cells". In: *Biophysical Journal* 78 (4 2000), pp. 1725–1735. DOI: 10.1016/S0006-3495(00)76724-5. URL: http://dx.doi.org/10.1016/S0006-3495(00)76724-5.

[112] Tomaso Poggio, Vincent Torre, and Christof Koch. "Computational vision and regularization theory". In: *Nature* 317.6035 (1985), pp. 314–319. DOI: 10.1038/317314a0. URL: http://dx.doi.org/10.1038/317314a0.

[113] D. Terzopoulos. "Regularization of Inverse Visual Problems Involving Discontinuities". In: *IEEE Transactions on Pattern Analysis and Machine Intelligence* PAMI-8.4 (1986), pp. 413–424. ISSN: 0162-8828. DOI: 10.1109/TPAMI.1986.4767807.

[114] S.I. Kabanikhin. "Definitions and examples of inverse and ill-posed problems". In: *J. Inv. Ill-Posed Problems* 16 (2008), pp. 317–357. ISSN: 0162-8828. DOI: 10.1515/JIIP.2008.069.

[115] Albert Tarantola. *Inverse Problem Theory and Methods and Models for Parameter Estimation*. Philadelphia, PA, USA: Society for Industrial and Applied Mathematics, 2005, pp. 1–37. ISBN: 0-89871-572-5.

[116] Mario Bertero and Patrizia Boccacci. *Introduction to Inverse Problems in Imaging*. Bath, UK: IOP Publishing Ltd, 1998, pp. 1–37. ISBN: 0 7503 0439 1.

[117] M. Bertero and M. Piana. "Inverse problems in biomedical imaging: modeling and methods of solution". In: *Complex Systems in Biomedicine*. Ed. by Alfio Quarteroni, Luca Formaggia, and Alessandro Veneziani. Milano: Springer Milan, 2006, pp. 1–33. ISBN: 978-88-470-0396-5. DOI: 10.1007/88-470-0396-2_1. URL: http://dx.doi.org/10.1007/88-470-0396-2_1.

[118] Andrew Thomas Delong. "Advances in Graph-Cut Optimization: Multi-Surface Models, Label Costs, and Hierarchical Costs [online]". Doctoral theses, Dissertations. The University of Western Ontario, London Ontario, Canada, 2011 [cit. 2016-09-19]. URL: http://www.psi.toronto.edu/~andrew/papers/thesis.pdf.

[119] David Waltz. "Understanding Line Drawings of Scenes with Shadows". In: *The Psychology of Computer Vision*. McGraw-Hill, 1975, pp. 19–91.

[120] Azriel Rosenfeld, Robert A. Hummel, and Steven W. Zucker. "Definitions and examples of inverse and ill-posed problems". In: *IEEE Transactions on Systems, MAN, and Cybernetics* 6.6 (1976), pp. 420–433.

[121] Katsuhiko Sakaue, Akira Amano, and Naokazu Yokoya. "Optimization Approaches in Computer Vision and Image Processing". In: *IEECE Trans. Inf. & Syst.* E82.3 (1999), pp. 534–547.

[122] Yuri Boykov, Olga Veksler, and Ramin Zabih. "Fast Approximate Energy Minimization via Graph Cuts". In: *IEEE Trans. Pattern Anal. Mach. Intell.* 23.11 (2001), pp. 1222–1239. ISSN: 0162-8828. DOI: 10.1109/34.969114. URL: http://dx.doi.org/10.1109/34.969114.

[123] Vladimir Kolmogorov. "Convergent Tree-Reweighted Message Passing for Energy Minimization". In: *Proc. Int'l Workshop Artificial Intelligence and Statistics*. 2005.

[124] David Mumford. "Optimal approximation by piecewise smooth functions and associated variational problems". In: *Commun. Pure Applied Mathematics* (1989), pp. 577–685.

[125] Jianbo Shi and Jitendra Malik. "Normalized Cuts and Image Segmentation". In: *IEEE Transactions on Pattern Analysis and Machine Intelligence* 22 (1997), pp. 888–905.

[126] T. Athanasiadis et al. "Semantic Image Segmentation and Object Labeling". In: *IEEE Transactions on Circuits and Systems for Video Technology* 17.3 (2007), pp. 298–312. ISSN: 1051-8215. DOI: 10.1109/TCSVT.2007.890636.

[127] Robert J. Adler and Jonathan E. Taylor. *Random fields and geometry*. Springer monographs in mathematics. New York: Springer, 2007. ISBN: 978-0-387-48112-8. URL: http://opac.inria.fr/record=b1123290.

[128] Anatoly V. Skorokhod Iosif I. Gikhman. *Introduction to the Theory of Random Processes*. Dover Books on Mathematics. Dover Publications, 1996. ISBN: 0486693872.

[129] Matthew Brett, Will Penny, and Stefan Kiebel. *An Introduction to Random Field Theory*. MRC Cognition and Brain Sciences Unit, Cambridge UK, 2003.

[130] Richard L. Smith. "Introduction to Besag (1974) Spatial Interaction and the Statistical Analysis of Lattice Systems". In: *Breakthroughs in Statistics*. Ed. by Samuel Kotz and Norman L. Johnson. New York, NY: Springer New York, 1997, pp. 285–323. ISBN: 978-1-4612-0667-5. DOI: 10.1007/978-1-4612-0667-5_13. URL: http://dx.doi.org/10.1007/978-1-4612-0667-5_13.

[131] Stuart Geman and Donald Geman. "Stochastic Relaxation, Gibbs Distributions, and the Bayesian Restoration of Images". In: *IEEE Trans. Pattern Anal. Mach. Intell.* 6.6 (1984), pp. 721–741. ISSN: 0162-8828. DOI: 10.1109/TPAMI.1984.4767596. URL: http://dx.doi.org/10.1109/TPAMI.1984.4767596.

[132] Julian Besag. "On the statistical analysis of dirty pictures". In: *Journal of the Royal Statistical Society B* 48.3 (1986), pp. 48–259.

[133] John Lafferty. "Conditional random fields: Probabilistic models for segmenting and labeling sequence data". In: Morgan Kaufmann, 2001, pp. 282–289.

[134] J. M. Hammersley and P. E. Clifford. "Markov random fields on finite graphs and lattices". In: Unpublished manuscript (1971).

[135] Gerhard Winkler. *Image Analysis, Random Fields and Markov Chain Monte Carlo Methods: A Mathematical Introduction (Stochastic Modelling and Applied Probability)*. Secaucus, NJ, USA: Springer-Verlag New York, Inc., 2006. ISBN: 3540442138.

[136] Cyril Cassisa. "Local Vs Global Energy Minimization Methods: Application to Stereo Matching". In: *IEEE* (2010), pp. 678–683. ISSN: 978-1-4244-6789-1.

[137] Olga Veksler. "Efficient Graph-based Energy Minimisation Methods in Computer Vision [online]". Doctoral theses, Dissertations. Cornell University, 1999 [cit. 2016-09-20]. URL: http://www.csd.uwo.ca/faculty/olga/Papers/thesis.pdf.

[138] V. Černý. "Thermodynamical approach to the traveling salesman problem: An efficient simulation algorithm". In: *Journal of Optimization Theory and Applications* 45.1 (1985), pp. 41–51. ISSN: 1573-2878. DOI: 10.1007/BF00940812. URL: http://dx.doi.org/10.1007/BF00940812.

[139] S. Kirkpatrick, C. D. Gelatt, and M. P. Vecchi. "Optimization by simulated annealing". In: *SCIENCE* 220.4598 (1983), pp. 671–680.

[140] L. A. MacEachern and T. Manku. "Genetic algorithms for active contour optimization". In: *Circuits and Systems, 1998. ISCAS '98. Proceedings of the 1998 IEEE International Symposium on*. Vol. 4. 1998, pp. 229–232. DOI: 10.1109/ISCAS.1998.698801.

[141] Lucia Ballerini. "Genetic Snakes for Medical Images Segmentation". In: *Evolutionary Image Analysis, Signal Processing and Telecommunications: First European Workshops, EvoIASP'99 and EuroEcTel'99, Göteborg, Sweden, May 26-27, 1999. Proceedings*. Ed. by Riccardo Poli et al. Berlin, Heidelberg: Springer Berlin Heidelberg, 1999, pp. 59–73. ISBN: 978-3-540-48917-7. DOI: 10.1007/10704703_5. URL: http://dx.doi.org/10.1007/10704703_5.

[142] Lucia Ballerini. "Genetic Snakes for Color Images Segmentation". In: *Applications of Evolutionary Computing: EvoWorkshops 2001: EvoCOP, EvoFlight, EvoIASP, EvoLearn, and EvoSTIM Como, Italy, April 18–20, 2001 Proceedings*. Ed. by Egbert J. W. Boers. Berlin, Heidelberg: Springer Berlin Heidelberg, 2001, pp. 268–277. ISBN: 978-3-540-45365-9. DOI: 10.1007/3-540-45365-2_28. URL: http://dx.doi.org/10.1007/3-540-45365-2_28.

[143] Reinhard Möller and Rene Zeipelt. "Automatic Segmentation of 3D-MRI Data Using a Genetic Algorithm". In: *Medical Imaging and Augmented Reality: First International Workshop, MIAR 2001, Hong Kong, China, June 10-12, 2001. Proceedings*. 2001, pp. 278–281. DOI: 10.1109/MIAR.2001.930303. URL: http://dx.doi.org/10.1109/MIAR.2001.930303.

[144] O. Ibáñez et al. "Genetic approaches for topological active nets optimization". In: *Pattern Recognition* 42.5 (2009), pp. 907–917. ISSN: 0031-3203. DOI: http://dx.doi.org/10.1016/j.patcog.2008.09.005. URL: http://www.sciencedirect.com/science/article/pii/S0031320308003762.

[145] Chris McIntosh and Ghassan Hamarneh. "Medical Image Segmentation: Energy Minimization and Deformable Models (Chapter 23)". In: *Medical Imaging: Technology and Applications* (2013). Ed. by T. Farncombe and K. Iniewski, pp. 661–692. URL: href="http://www.cs.sfu.ca/~hamarneh/ecopy/crc2013a.pdf">.

[146] D. Terzopoulos. "On matching deformable models to images". In: *Optical Society of America, Topical Meeting on Machine Vision*. Provided by the SAO/NASA Astrophysics Data System. 1987. URL: http://adsabs.harvard.edu/abs/1980osa..meet..160T.

[147] T. F. Chan and L. A. Vese. "Active Contours Without Edges". In: *Trans. Img. Proc.* 10.2 (2001), pp. 266–277. ISSN: 1057-7149. DOI: 10.1109/83.902291. URL: http://dx.doi.org/10.1109/83.902291.

[148] Judea Pearl. *Probabilistic Reasoning in Intelligent Systems: Networks of Plausible Inference.* San Francisco, CA, USA: Morgan Kaufmann Publishers Inc., 1988. ISBN: 0-934613-73-7.

[149] Brendan Frey and David MacKay. "A Revolution: Belief Propagation in Graphs With Cycles". In: *In Neural Information Processing Systems.* MIT Press, 1998, pp. 479–485.

[150] William T. Freeman, Egon C. Pasztor, and Owen T. Carmichael. "Learning Low-Level Vision". In: *Int. J. Comput. Vision* 40.1 (2000), pp. 25–47. ISSN: 0920-5691. DOI: 10.1023/A:1026501619075. URL: http://dx.doi.org/10.1023/A:1026501619075.

[151] Vladimir Kolmogorov and Ramin Zabih. "What energy functions can be minimized via graph cuts?" In: *IEEE Transactions on Pattern Analysis and Machine Intelligence* 26.2 (2004), pp. 65–81.

[152] Y. Boykov and M.P. Jolly. "Interactive graph cuts for optimal boundary and region segmentation of objects in N-D images". In: *Proc. IEEE Int'l Conf. on Computer Vision* 1 (2001), pp. 105–112.

[153] Yuri Boykov and Vladimir Kolmogorov. "An Experimental Comparison of Min-Cut/Max-Flow Algorithms for Energy Minimization in Vision". In: *IEEE Transactions on Pattern Analysis and Machine Intelligence* 26 (2001), pp. 359–374.

[154] Vladimir Kolmogorov et al. "A Comparative Study of Energy Minimization Methods for Markov Random Fields with Smoothness-Based Priors". In: *IEEE Transactions on Pattern Analysis & Machine Intelligence* 30.undefined (2007), pp. 1068–1080. ISSN: 0162-8828. DOI: doi.ieeecomputersociety.org/10.1109/TPAMI.2007.70844.

[155] P. Kohli, M. Pawan Kumar, and P. H. S. Torr. "P^3 & Beyond: Move Making Algorithms for Solving Higher Order Functions". In: *IEEE Transactions on Pattern Analysis and Machine Intelligence* 31.9 (2009), pp. 1645–1656. ISSN: 0162-8828. DOI: 10.1109/TPAMI.2008.217.

[156] Nikos Komodakis, Georgios Tziritas, and Nikos Paragios. "Fast, Approximately Optimal Solutions for Single and Dynamic MRFs". In: *CVPR.* IEEE Computer Society, 2007. ISBN: 1-4244-1179-3. URL: http://dblp.uni-trier.de/db/conf/cvpr/cvpr2007.html#KomodakisTP07.

[157] M. Pawan Kumar and Daphne Koller. "MAP Estimation of Semi-metric MRFs via Hierarchical Graph Cuts". In: *Proceedings of the Twenty-Fifth Conference on Uncertainty in Artificial Intelligence.* UAI '09. Arlington, Virginia, United States: AUAI Press, 2009, pp. 313–320. ISBN: 978-0-9749039-5-8. URL: http://dl.acm.org/citation.cfm?id=1795114.1795151.

[158] D. M. Greig, B. T. Porteous, and A. H. Seheult. "Exact Maximum A Posteriori Estimation for Binary Images". In: *Journal of the Royal Statistical Society. Series B (Methodological)* 51.2 (1989), pp. 271–279. ISSN: 00359246. URL: http://www.jstor.org/stable/2345609.

[159] Sébastien Roy and Ingemar Johansson Cox. "A maximum-flow formulation of the n-camera stereo correspondence problem". In: *Computer Vision, 1998. Sixth International Conference on.* 1998, pp. 492–499.

[160] Yuri Boykov, Olga Veksler, and Ramin Zabih. "Markov Random Fields with Efficient Approximations." In: *CVPR.* IEEE Computer Society, 1998, pp. 648–655. ISBN: 0-8186-8497-6. URL: http://dblp.uni-trier.de/db/conf/cvpr/cvpr1998.html#BoykovVZ98.

[161]   L. R. Ford and D. R. Fulkerson. "Maximal Flow through a Network". In: *Canadian Journal of Mathematics* 8 (1956), pp. 399–404. URL: http://www.rand.org/pubs/papers/P605/.

[162]   E.A. Dinic. "Algorithm for solution of a problem of maximum flow in a network with power estimation". In: *Soviet Math* 11 (1970), pp. 1277–1280.

[163]   Jack Edmonds and Richard M. Karp. "Theoretical Improvements in Algorithmic Efficiency for Network Flow Problems". In: *J. ACM* 19.2 (1972), pp. 248–264. ISSN: 0004-5411. DOI: 10.1145/321694.321699. URL: http://doi.acm.org/10.1145/321694.321699.

[164]   Andrew V. Goldberg and Robert E. Tarjan. "A New Approach to the Maximum-flow Problem". In: *J. ACM* 35.4 (1988), pp. 921–940. ISSN: 0004-5411. DOI: 10.1145/48014.61051. URL: http://doi.acm.org/10.1145/48014.61051.

[165]   Narsingh Deo. *Graph Theory with Applications to Engineering and Computer Science (Prentice Hall Series in Automatic Computation)*. Upper Saddle River, NJ, USA: Prentice-Hall, Inc., 1974. ISBN: 0133634736.

[166]   John Adrian Bondy. *Graph Theory With Applications*. Oxford, UK, UK: Elsevier Science Ltd., 1976. ISBN: 0444194517.

[167]   Maarten van Steen. *Graph theory and complex networks : An introduction*. Lexington: Maarten van Steen, 2010. ISBN: 978-90-815406-1-2. URL: http://opac.inria.fr/record=b1130915.

[168]   Mark Newman. *Networks: An Introduction*. 1st edition. Oxford University Press, 2010. ISBN: 0199206651.

[169]   Eugene Lawler. "4.5. Combinatorial Implications of Max-Flow Min-Cut Theorem, 4.6. Linear Programming Interpretation of Max-Flow Min-Cut Theorem". In: *Combinatorial Optimization: Networks and Matroids*. Ed. by Eugene Lawler. Dover, 2001, pp. 117–120. ISBN: 0-486-41453-1.

[170]   Solomon Eyal Shimony. "Finding MAPs for belief networks is NP-hard". In: *Artificial Intelligence* 68.2 (1994), pp. 399–410. ISSN: 0004-3702. DOI: http://dx.doi.org/10.1016/0004-3702(94)90072-8. URL: http://www.sciencedirect.com/science/article/pii/0004370294900728.

[171]   Thomas H. Cormen et al. *Introduction to Algorithms, Third Edition*. 3rd. The MIT Press, 2009. ISBN: 0262033844, 9780262033848.

[172]   V. B. Cherkassky and V. A. Goldberg. "On Implementing the Push—Relabel Method for the Maximum Flow Problem". In: *Algorithmica* 19.4 (19), pp. 390–410. ISSN: 1432-0541. DOI: 10.1007/PL00009180. URL: http://dx.doi.org/10.1007/PL00009180.

[173]   R. Szeliski et al. *A Comparative Study of Energy Minimization Methods for Markov Random Fields with Smoothness-Based Priors*. 2008. DOI: 10.1109/TPAMI.2007.70844.

[174]   Nhat Bao Sinh Vu. "Image Segmentation with Semantic Priors: A Graph Cut Approach [online]". Doctoral theses, Dissertations. University of California, Santa Barbara, 2008 [cit. 2016-10-03]. URL: https://vision.ece.ucsb.edu/sites/vision.ece.ucsb.edu/files/publications/NhatsThesis.pdf.